Design Study of a Three-Wheeled Urban Electric Vehicle

by

Harry L. Zheng

A thesis

presented to the University of Waterloo

in fulfillment of the

thesis requirement for the degree of

Master of Applied Science

in

Mechanical Engineering

Waterloo, Ontario, Canada, 2014

AUTHOR'S DECLARATION

I hereby declare that I am the sole author of this thesis. This is a true copy of the thesis, including any required final revisions, as accepted by my examiners. I understand that my thesis may be made electronically available to the public.

Abstract

This thesis documents the development study of a three-wheeled electric urban vehicle through its initial design stages, which includes needs analysis, development of rough order-of-magnitude calculations, and concept design. To account for limited time and resources, the scope of design considerations is restricted to ergonomics, linear performance, cornering dynamics and crashworthiness. In the needs analysis stage, the requirements in each area of consideration are investigated, culminating in a set of specifications. Rough order-of-magnitude calculations were then developed to check specification compliance of potential concepts. Finally, a concept is designed to demonstrate application of the initial calculations.

Acknowledgements

I would like to thank my supervisor, Professor Amir Khajepour, for creating this opportunity for me to learn in a flexible manner, and for introducing me to the world of vehicle dynamics.

I would also like to thank Professor Oscar Nespoli for his participation in my thesis committee as well as his valuable instruction on design methodology taught as part of the Design Certificate Program at the University of Waterloo, I hope the insightful way of thinking that I have learned from this course will be reflected in every design I make for the rest of my career.

Finally, I extend my thanks to colleagues Professor Avesta Goodarzi, Professor Alireza Kasaiezadeh, Amir Soltani, Alireza Pazooki, Adrian Wong, Masoud Ansari, Liu Huan, and Ji Jie for their kind assistance and friendship.

Dedication

I dedicate this thesis to my parents, who supported me through the challenging process of its completion

Table of Contents

List of Figures

List of Tables

Chapter 1
Introduction

1.1 Background

An urban vehicle is a small vehicle designed for urban commuting. The term “urban vehicle” used in this thesis refers to vehicles that are much smaller than the average passenger car. Depending on the jurisdiction, such vehicles may be classified as city cars, micro cars, quadricycles, or other similar designation.

Compared to average passenger vehicles, urban vehicles are able to navigate and park in cluttered urban centers with greater ease. In addition, large-scale adoption of urban vehicles could potentially ease traffic congestion faced by many cities today.

Two difficulties arise if urban vehicles are to be made even smaller in the future. First, a smaller vehicle size also means the space between the wheels become smaller and occupants sit more upright, resulting in a loss of dynamic stability. Second, the reduction in size also means a reduction in space available for crash structures, which are needed to ensure occupant safety.

Three urban vehicle technologies are currently under development at the Mechatronic Vehicle Laboratory at the University of Waterloo as possible answers to these challenges. The first is a highly compact wheel module capable of artificially increasing wheel track by actively cambering the tires up to large angles. The second is a metal foam crash structure that can be crushed at a more controllable rate compared to conventional crash structures, thus generating a more even deceleration under crash conditions and improving crash safety. The third is an electronic drive-by-wire system that aids the driver in avoiding collisions.

The subject of this thesis is on the design of an urban vehicle to serve as a test bed for these technologies. Should the viability of these technologies be demonstrated, there is a possibility that the vehicle will be further developed into a production version intended for the mainstream market. The project and core technologies will be discussed in more detail below.

1.2 Core Technologies

1.2.1 Corner Wheel Module

In conventional cars, the wheel, suspension, steering and drivetrain are separate systems that work together to generate the desired vehicle motion. Such a configuration takes up significant space and does not permit the steer, camber, and vertical displacement of the wheels to be kinematically independent.

The corner wheel module (CWM) incorporates all of the above systems into a single, compact module that is fully symmetric for installation on any wheel mounting point. The module incorporates steer-by-wire, in-wheel suspension, and a built-in motor so that it does not require any mechanical linkage to function. In addition, it features an Active Camber function that allows for control of wheel camber in addition to steering. With the CWM, the usable interior space and dynamic stability of future urban vehicles may be improved significantly.

1.2.2 Metal Foam Crash Structure

A serious drawback of urban vehicles and small cars in general is the limited size of their crumple zones for crash safety. One way to mitigate this issue is to improve the crush efficiency of the crumple zone such that ratio between maximum and mean cabin impact accelerations is minimized. By reducing maximum acceleration throughout impact, the likelihood of serious occupant injury is decreased.

In conventional cars, the crumple zone is populated by numerous components of various mechanical properties such that the cabin is decelerated unevenly as each component deforms upon impact. Recent research [1] [2] has shown that metal foams can be incorporated into the crash structure for a more even cabin deceleration during impact. If highly compact components are incorporated into an urban vehicle, it is possible to maximize the metal foam content in its crash structure for enhanced crumple efficiency.

1.2.3 Active Safety System

In contrast to passive crash mitigation, which is aimed at reducing impact forces on the occupant, active crash mitigation is an attempt to completely avoid any collision. Numerous

such technologies, such as Anti-Lock Braking, Traction Control, and Collision Avoidance System are already in existence. The Urban Active Safety System builds upon these technologies to further enhance their effectiveness under urban driving environments, where road clutter is significant and reflexes are more heavily taxed. Such a system would require advanced control algorithms to determine the best course of action in an imminent collision, with due consideration for road clutter and dynamic limitations of the parent vehicle.

1.3 Thesis Scope and Structure

The long-term goal of the project is to design and build an urban vehicle concept to serve as a test bed and demonstrator for the technologies described above. The process of designing such a vehicle is long and elaborate, especially if commercialization is considered.

A general process for engineering design [3] consists of needs analysis, conceptual design, embodiment design, and detailed design (Figure 1). Needs analysis, which is required in virtually all engineering design projects, involves generation of specifications that must be consistently fulfilled by the product throughout all stages of its evolution. To encourage innovation, there is often a conceptual design stage where numerous possibilities for the final product are explored and a winning proposal selected. In the embodiment design stage, the selected concept undergoes further refinement, with block representations of actual components arranged into a feasible package. Components become progressively more detailed as the design transitions to the detailed design stage up to project completion. Throughout the entire design process, analyses are performed to continuously check the design's compliance with design requirements. During the early stages of design, these analyses may be in the form of rough order-of-magnitude (ROM) calculations, which provide quick estimates of key vehicle parameters using limited information and sweeping assumptions. As the design matures, these ROM calculations are either improved or replaced by more sophisticated models like finite element analysis, multi-body dynamics, and computational fluid dynamics.

Due to limited time and resources, the scope of this thesis will be restricted to needs analysis, development of ROM calculations, and the design of a partial concept, covered in Chapter 2, Chapter 3 and Chapter 4, respectively. In addition to design stages, the scope is also restricted in terms of aspects of vehicle design considered. In a real-world vehicle

design project, for example, the number of specifications developed can be in the hundreds or even thousands, spanning areas such as regulations, ergonomics, lighting, noise-vibration-harshness, performance, dynamics, manufacturing, industrial design, crashworthiness, electrical systems, and much more. In this thesis, only ergonomics, linear performance, turning dynamics and crashworthiness will be considered in detail.

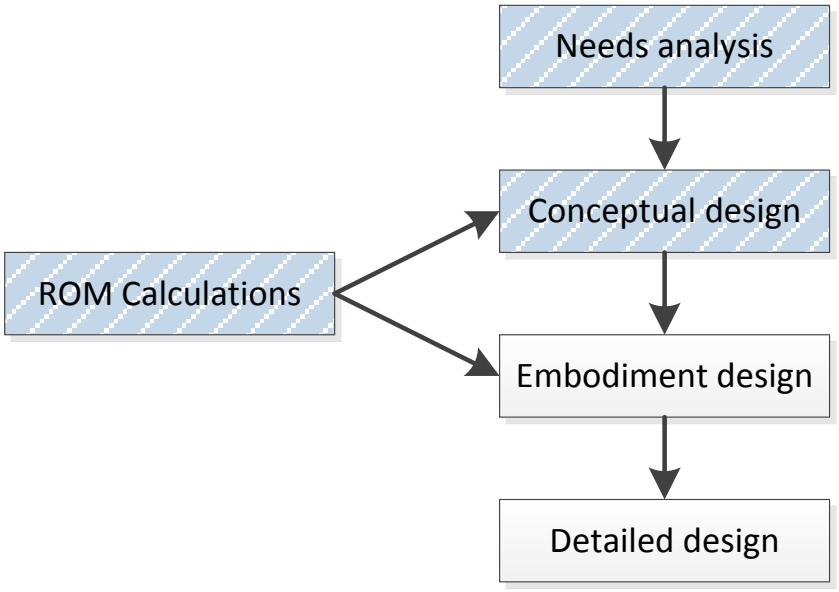

Figure 1 – A general process for engineering design, showing stages that are partially completed in this thesis

In the next chapter, we begin the needs analysis stage by evaluating vehicle requirements and generating specifications.

Chapter 2
Requirements and Specifications

In this chapter, specifications are developed to serve as guidelines for the project. These specifications are either directly given by stakeholders, or derived from their needs through further investigation. It should be noted that due to limited time and resources, the list of specifications developed in this thesis is non-exhaustive, and the definitions of some specifications are rudimentary. As the project progresses beyond the scope of this thesis, the specifications are expected to increase in numbers and refinement.

This chapter is divided into three sections. In Section 2.1, the stakeholders, whose requirements the vehicle must satisfy are identified. In Sections 2.2 and 2.3, stakeholder requirements are further refined into vehicle form and performance specifications, respectively.

2.1 Identification of Stakeholders

In the context of requirements engineering, a stakeholder is an individual or party that has an interest in the project and expectations on how the final product should perform. The main stakeholders for the current project are the technology developers responsible for developing the CWM, crash structure, and active safety system. Their general requirements for the project vehicle is that first, it must be able to incorporate their technologies for testing and demonstration, and second, it must partially satisfy consumer and legal requirements to facilitate possible transition into a production vehicle. The latter requirement means consumers and regulatory bodies are indirect stakeholders of the project.

2.2 Form Requirements

2.2.1 Wheel Arrangement

A three-wheel configuration was specified by the technology developers as a design requirement to showcase the benefits of the new technologies. All else the same, a three-wheel configuration is inherently less stable than a four-wheel configuration. However, since

the purpose of the CWM is to enhance stability during cornering, successful implementation of this technology on a three-wheel vehicle would serve to demonstrate its viability.

2.2.2 Corner Wheel Module Integration

The need to integrate the CWMs into the project vehicle leads to further requirements in terms of propulsion, steering, and energy storage.

Since each CWM is powered by a built-in electric motor, the overall method of propulsion for the vehicle must be through these electric motors. The performance parameters of the motors are customizable and need to be selected based on the performance envelope of the vehicle.

The steering and camber mechanism of the motors are electrically actuated. Therefore, there should be no mechanical linkages between the CWMs and driver.

Energy storage should be in the form of lithium-ion batteries. These batteries were selected by the technology developers because of their performance and commercial availability. The battery system must be designed to satisfy the electrical needs of the motors.

2.2.3 Seating Capacity and Arrangement

The vehicle must seat two occupants in a side-by-side arrangement. This arrangement was specified by the technology developers as an alternative to tandem arrangements found on narrow-body urban vehicles such as the Nissan Land Glider. The advantages of a side-by-side arrangement is that first, it would facilitate communication between the occupants, and second, it eliminates the need for full-body tilting during cornering, thus reducing complexity and improving the safety of storing liquid refreshments onboard.

2.2.4 Occupant Space

As a car for everyday use, the project vehicle should be designed to accommodate occupants of mainstream body sizes comfortably. A common upper bound for maximum accommodated body size is 95^{th} percentile US male [4]. SAE standards J1052 and J4004 from the SAE handbook [5] can be used as guidelines for occupant packaging.

2.2.5 Outer Dimensions

The outer dimensions of the vehicle are considered in two cases: with all doors closed or all doors open. Dimensional requirements for the doors-closed case will be derived based on traffic flow considerations, while that for the doors-open case will be derived based on parking considerations.

Studies have shown that smaller vehicles have a favorable impact on traffic flow due to the reduction in headway [6]. Using a signalized urban traffic model, one study found that traffic flow can be improved by as much as 70% if vehicle lengths are halved from 6.1 m to 3.06 m (Table 1).

Table 1 – Impact of small cars on traffic flow [7]

Percent small cars[1]	Flow (vehicles/h)[2]	Velocity (km/h)
0%	732	3.8
10%	745	3.7
33%	855	4.4
50%	1005	4.9
100%	1240	6.0

[1]Small and large cars have lengths of 3.05 and 6.1 m, respectively.

[2]Vehicles per hour of green light

Vehicle length has the largest impact on traffic flow. Width can play a role as well if the vehicle is narrow enough for lane-splitting or travel on special narrow lanes, although this will be subject to infrastructural and legal restrictions in North America. Nevertheless, width does play a more important role in ease of parking, as will be discussed later in this section.

Due to a lack of design constraints at this stage, the specification for vehicle length will not be hard, quantitative targets. A soft target for length would be that the vehicle must be as short as possible without compromising other requirements, the most important of which are packaging, dynamics, and crashworthiness. Using the same approach, vehicle height is defined in the same way.

A numerical target for maximum vehicle width (including possible added width due to open doors) can be specified based on the width of parking spaces. Since the project vehicle is

optimized for urban use, it must be sufficiently narrow to provide comfortable clearance between itself and other parked cars. Parking spaces are sized using design vehicles, which are about 2030 mm wide [8]. The actual widths of parking stalls vary between 8’ 3” (~2500 mm) and 9’ (~2700 mm) [9]. To maximize comfort, no part of the project vehicle – with all doors open – should protrude into neighbouring parking spaces or the wall. In addition, the vehicle body itself must be as narrow as possible to provide maximum clearance between the vehicle and parking stall boundaries.

In summary, the length, width and height of the vehicle with all doors closed should be as small as possible without compromising packaging, dynamic and crashworthiness requirements. With all doors open, vehicle width should not exceed 2500 mm.

2.2.6 Ground Clearance Heights and Angles

This section concerns the clearance of the vehicle over obstacles such as potholes, bumps, curbs and ramps. Three heights and three angles are of interest: the front bumper, rear bumper and ground clearance heights and the approach, departure, and ramp-over angles (Figure 2).

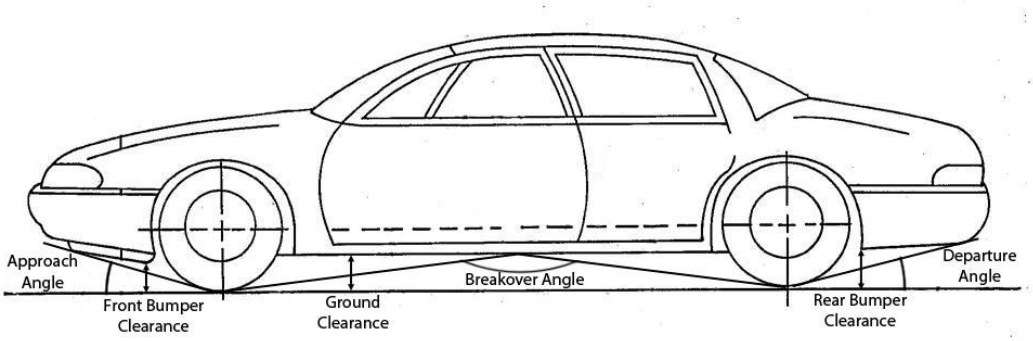

Figure 2 – Clearance heights and angles (adapted from SAE Handbook Standard J689) [5]

Ground, front bumper, and rear bumper clearances are defined as the minimum distance between the ground and the bottom of the vehicle main body, front overhang, and rear overhang, respectively. Bumper height clearances are important for clearing objects that the car does not normally drive over, such as parking space wheel blocks. Ground clearance is

important for obstacles that are frequently driven over, such as speed bumps. Speed bumps typically have a height of 3 to 6 inches (76 to 152 mm) [10]. Thus, a ground clearance of 160 mm would be sufficient.

Approach angle is defined the minimum angle between the ground and a line that is both tangent to the statically loaded front tire and coincident with the lower part of the front vehicle body. Departure angle is defined the same way but with the rear tire and lower part of the rear body. Break-over angle is the maximum possible angle formed by two lines, one tangent to the front tire and one tangent to the rear tire, intersecting at a point on the bottom of the vehicle body. These angles need to be large enough for the vehicle to climb short ramps such as those on tow trucks and car carriers without scraping the ramp with the bottom of its nose, midsection, or tail.

Recommended minimum values for the above clearances are given in SAE standard J689 (Table 2) [5]. The minimum recommended front/rear bumper clearance is consistent with the AASHTO standard for maximum curb height of 150 to 200 mm [11]. Clearance angle recommendations are set based on clearance requirements of car carrier ramps [5]. A statistic review of vehicle dimensions based on 5140 vehicles measured by NHTSA [12] shows that the majority of vehicles exceed the 203 mm bumper clearance height by a significant amount (Figure 3 a and b). The same data for approach angle (Figure 3 c)) shows that a number of vehicles are below the 16 degree recommendation, although the data does not show whether angles are measured to deformable non-structural components, which are permitted to contact the ramp under SAE J689.

The SAE recommendations will be adopted as the minimum clearance specifications of the project vehicle. Where possible, these should be exceeded by a small safety factor.

Table 2 – Recommended clearances from SAE Standard J689 [5]

Approach angle	16 degrees
Departure angle	13 degrees
Front/rear bumper clearance	203 mm
Ramp-over angle	12 degrees

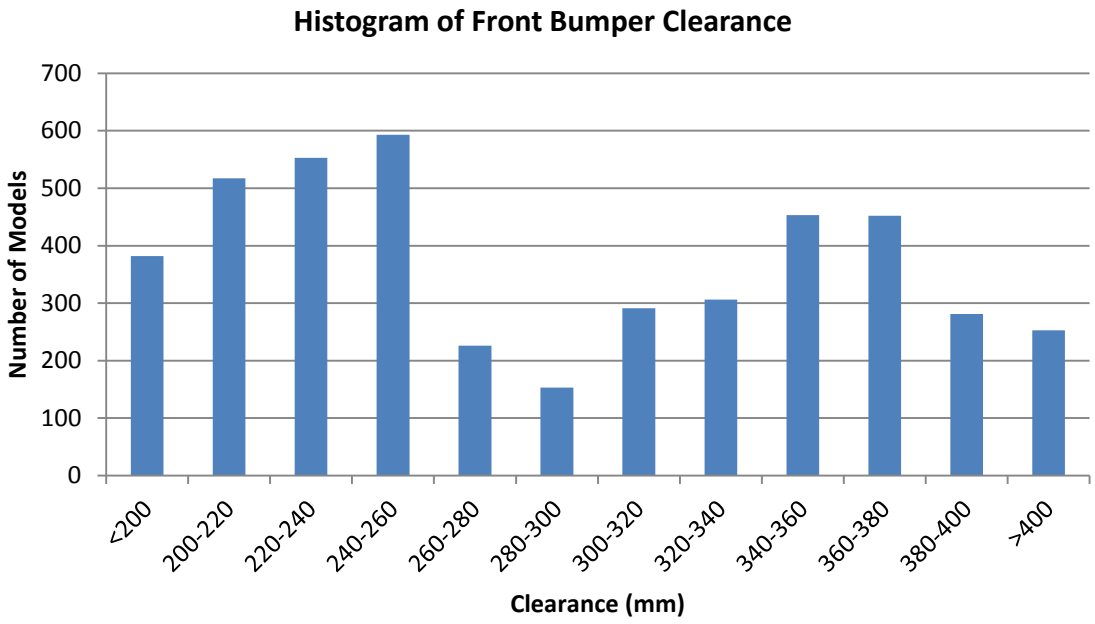
Histogram of Front Bumper Clearance
Number of Models
700
600
500
400
300
200
100
0
<200
200-220
220-240
240-260
260-280
280-300
300-320
320-340
340-360
360-380
380-400
>400
Clearance (mm)

a)

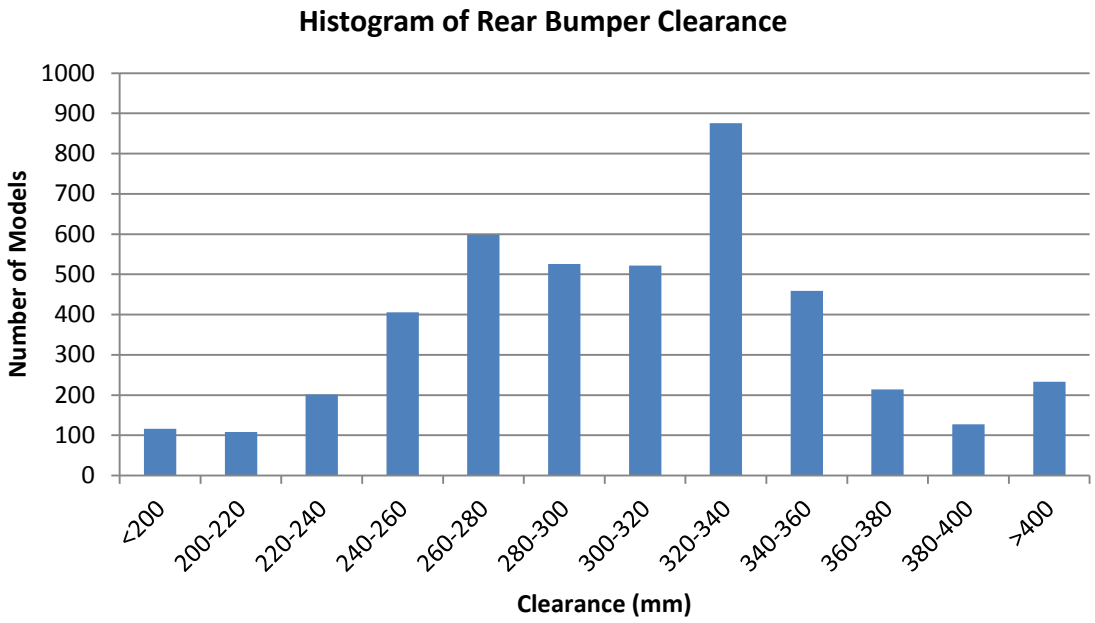
Histogram of Rear Bumper Clearance
Number of Models
1000
900
800
700
600
500
400
300
200
100
0
<200
200-220
220-240
240-260
260-280
280-300
300-320
320-340
340-360
360-380
380-400
>400
Clearance (mm)

b)

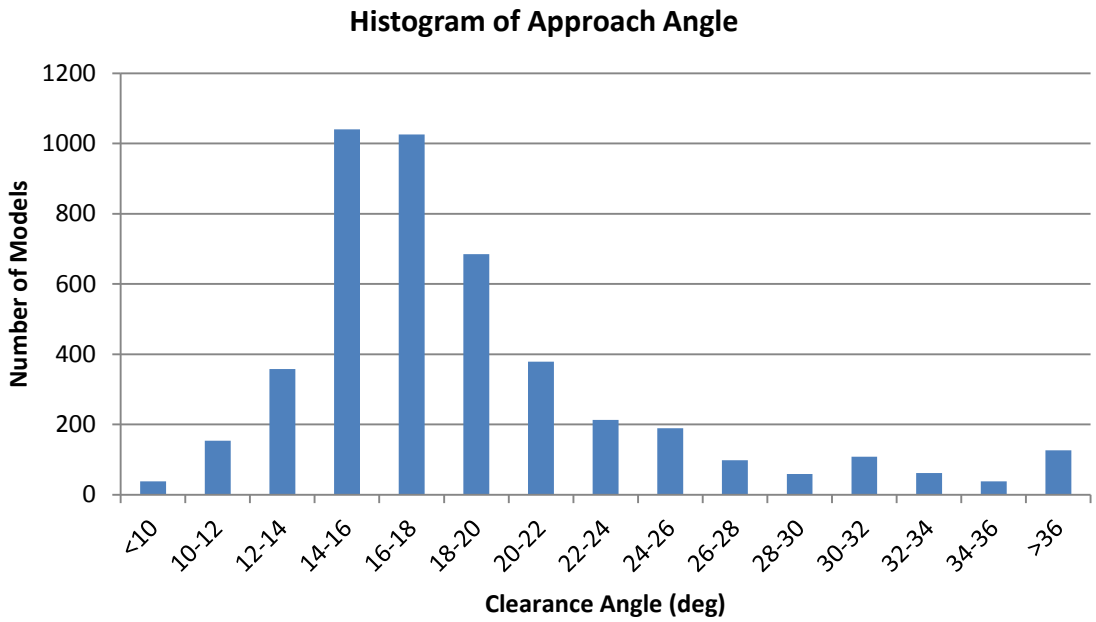

c)

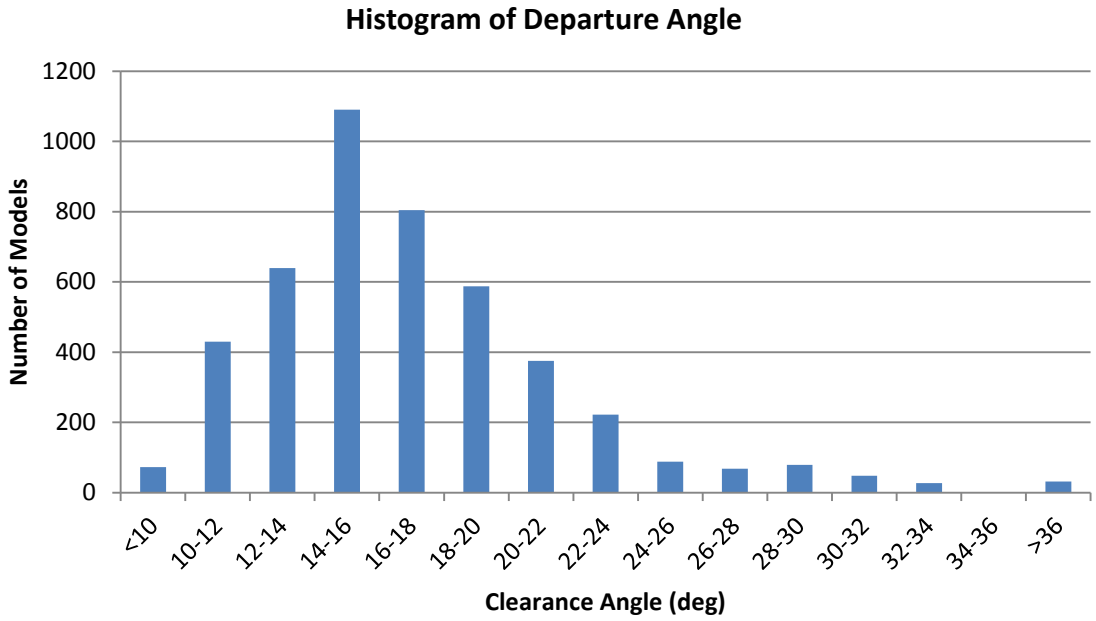

d)

Figure 3 – Histogram of a) front bumper clearance, b) rear bumper clearance, c) approach angle and d) departure angle based on NHTSA database of 5140 car models produced between 1977 and 2000 [12]

2.3 Performance Requirements

2.3.1 Linear Performance

2.3.1.1 Maximum Range

The urban vehicle should have sufficient range to satisfy the daily travel distance of the majority of the population. A literature review of studies on travel distance and range preference was conducted by Franke [13] and shown on Table 3 and Table 4, respectively. The results of these studies suggest that daily travel distance in the US and Europe seldom exceed 100 km.

Interestingly, various surveys reveal that motorists tend to expect much greater range in a vehicle than what they actually need on a typical day. Table 4 shows minimum range preferences anywhere from 200 km to over 400 km. One reason for this discrepancy may be because aside from daily trips, long distance trips in excess of 100 km are in fact taken on several days of the year, as can be seen from the findings of Pearre et. al. [14] on Table 3. Despite this, it should be stressed that the purpose of the urban vehicle is exclusively to provide a means for door-to-door urban transportation at minimum cost, thus it does not need to be capable of making these long trips.

One additional consideration for range specification is the way that range is measured. Range can vary greatly depending on factors such as terrain, driving style and electrical equipment use. To measure range and energy consumption in a standardized way, drive cycles were developed by various institutions. One drive cycle that is particularly suitable for the urban vehicle is the New York City Cycle (NYCC), which simulates heavy stop-and-go traffic frequently encountered in urban environments. Aside from using a drive cycle, range measurement should also be conducted with onboard electrical equipment such as air conditioners or heaters turned on.

Finally, a margin of safety should be added to the range specification. From Table 3, it would appear that a range of 100 km will satisfy the needs of 85 to 95% of the population. Adding a 10 km margin of safety, the range specification of the urban vehicle shall be stated as 110 km under the NYCC.

Table 3 – Survey of daily driving distance [13]

Study	Sample size and location	Results
Infas and DLR, 2010 [15]	60,713; Germany	Average 39 km per day
Zumkeller et al., 2011 [16]	1800; Germany	Average 41 km per day
Oko-Institut, 2011 [17]	Germany	80th percentile: 50 km per day 95th percentile: 100 km per day Average 12 trips per year of distance >160 km
TUV Rheinland, 2011 [18]	1000; Germany	61st percentile: 50 km per day 91st percentile: 100 km per day
Bunzeck et al., 2011 [19]	1899; 7 EU countries	24% drive <20 km 61% drive between 21-100 km
Giffi et al., 2011 [20]	>13,000; 17 countries worldwide	78th percentile: 80 km per day (Germany)
Pearre et al., 2011 [14]	484; Atlanta, Georgia	Average: 45 miles (72 km) per day Median: 30 miles (48 km) per day Exceeds 161 km on average of 23 days/year Exceeds 241 km on average of 9 days/year
Krumm, 2012 [21]	150,147; US	Average: 38.4 miles (61.8 km) per day

Table 4 – Survey of vehicle range preference [13]

Study	Sample size and location	Results
VDE, 2010 [22]	1000; Germany	Average 353 km
ADAC, 2013 [23]	803; Germany (ADAC members)	2011: 74% prefers more than 200 km 2013: 50% prefers more than 200 km
Bunzeck et al., 2011 [19]	1899; 7 EU countries	Average 308 km (Europe) Average 328 km (Germany)
Giffi et al., 2011 [20]	>13,000; 17 countries worldwide	60% prefers more than 320 km (Germany)
Bronchard et al., 2011 [24]	7003; 12 countries worldwide	Average 437 km
Zpryme, 2010 [25]	1046; US	Average 294 miles
Krumm, 2012 [21]	150,147; US	60 mile (97 km) range EV satisfies 83% 80 mile (129 km) range EV satisfies 90% 120 mile (193 km) range EV satisfies 95%

2.3.1.2 Speed-Acceleration Profile

The speed-acceleration profile is important for ensuring that the vehicle is capable of keeping up with traffic, both in terms of maximum speed and acceleration from standstill. In addition, the speed-acceleration profile of the vehicle must also cover the profile found in standard drive cycles to ensure that it is capable of executing the drive cycle for the purpose of obtaining energy consumption data. To produce the required speed-acceleration profile, it is necessary to examine the maximum speed required for city driving, the speed-acceleration profile of a selected drive cycle, and the acceleration profiles of typical cars.

With respect to speed, it should be recognized that as a vehicle designed exclusively for urban commuting at minimal cost, the project vehicle does not need to be capable of driving on highways, since such a capability will add cost, weight, and size. The fastest roads that the vehicle should be designed for are urban arterial roads, as defined by the American

Association of State Highway Transportation Officials (AASHTO) [11], which are designed for running speeds of 30-75 km/h. For contingency, the maximum speed of the vehicle should thus be 80 km/h.

The acceleration profile of the vehicle should encompass that of the NYCC drive cycle as well as profiles encountered in actual driving conditions. The speed-acceleration profile of the NYCC drive cycle is shown on Figure 4, with a dotted line showing the minimum acceleration profile necessary to execute this drive cycle. Results from traffic studies on the acceleration behaviors of drivers are shown on Figure 5 and Figure 6.

The required acceleration profile of the vehicle is shown on Figure 7. Note that this profile has the same shape as the torque-speed curve of a typical DC motor. To ensure efficiency, the motor should be selected such that it operates at highest efficiency when the vehicle is cruising at 50-80 km/h.

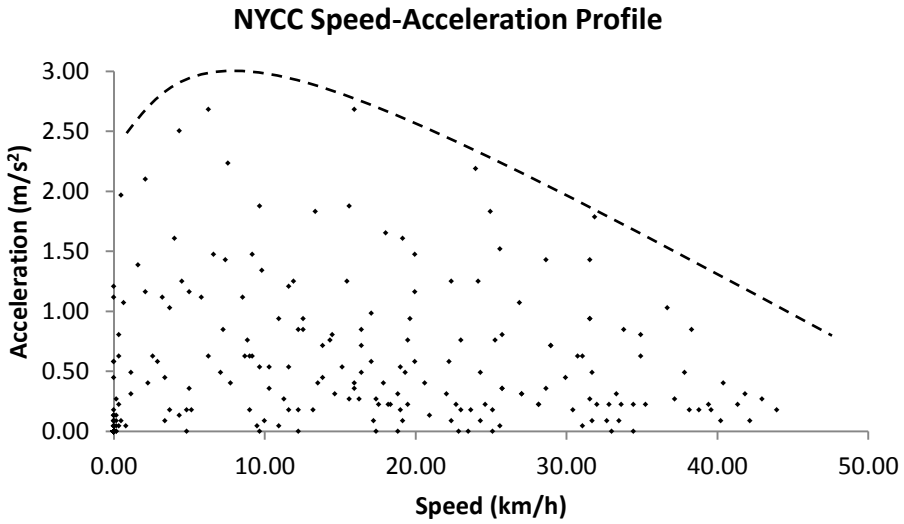

Figure 4 – Speed-acceleration profile of the NYCC drive cycle

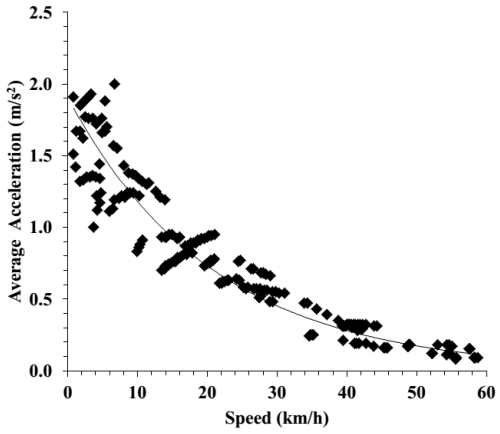

Figure 5 – Acceleration profiles observed on passenger cars on a 4-lane highway [26]

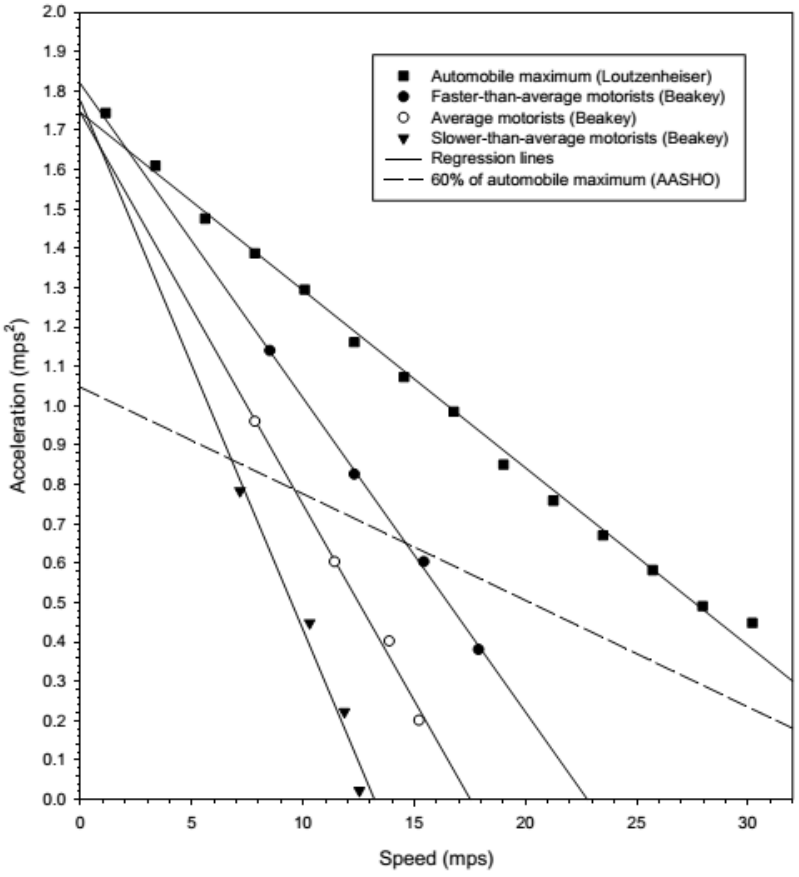

Figure 6 – Acceleration behavior of slower, average, and faster drivers [27]

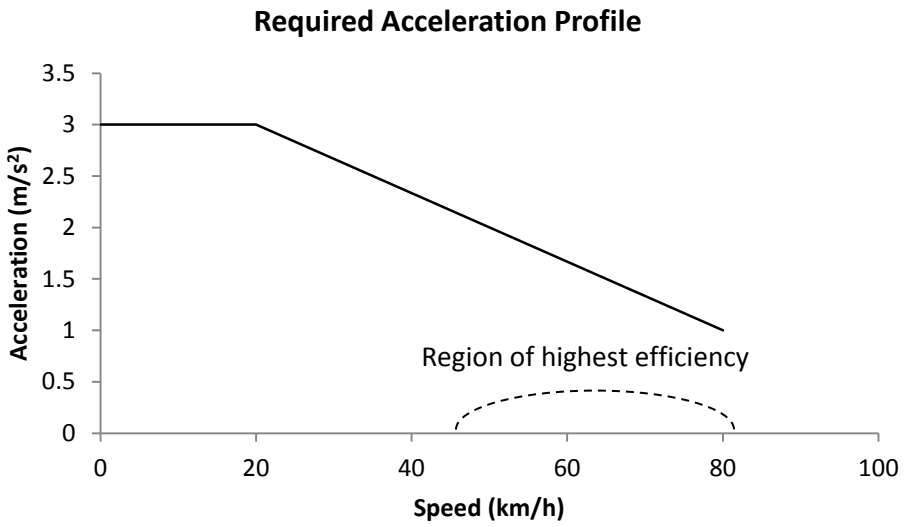

Figure 7 – The required acceleration profile of the project vehicle

2.3.1.3 Gradability

Gradeability is a measure of the hill-climbing ability of a vehicle. The gradient of a road is defined as its rise in elevation over a specified horizontal span. For example, a road that rises by 10 m over a horizontal span of 100 m has a gradient of 10%. A vehicle's rectilinear performance is adversely affected by upward gradient. Without adequate torque from its powertrain, a vehicle will have trouble keeping up with traffic or even sustaining forward motion on steep gradients.

There are two useful ways of defining gradeability: one is the maximum gradient at which a vehicle can sustain a certain speed; the other is the maximum gradient at which a vehicle can sustain forward motion. In this thesis, they will be referred to as at-speed gradability and stall-speed gradability, respectively. At-speed gradability is applicable when driving on public roads, where gradients are usually small but a certain speed must be maintained in order to keep up with traffic. Stall-speed gradability is applicable when climbing up steep ramps such as those in parking complexes, where the ability to climb rather than speed is of importance. To determine gradeability requirements for the project vehicle, regulations and guidelines for road and ramp design will be examined.

According to AASHTO guidelines [11], the maximum gradient of urban roads should not exceed 15% for residential areas and 8% for commercial and industrial areas. Furthermore, the maximum design grade for a road with a design speed of 50 km/h should be no more than 12%. The latter requirement will be used for the at-speed gradability of the vehicle at 50 km/h, and speeds for even higher grades are assumed to be much lower. Taking into consideration the performance deterioration of batteries at lower states of charge, measures should be taken to ensure that this at-speed gradability is maintained so long as battery state of charge is above 30% (the battery should power off below this state of charge to prevent damage from excessive discharge).

The maximum possible gradient encountered by the vehicle can be found in parking structures. According to parking garage design guidelines, maximum non-parking ramp grades should be in the range of 12-14%, although grades up to 20% are possible [9]. Adding some contingency, the stall-speed gradability of the vehicle should thus be 25%

2.3.2 Turning Performance

2.3.2.1 Minimum Turn Radius

The ability to make extremely tight turns is desirable for future urban vehicles, as it makes parking and navigation through cluttered roads much easier. With a sufficiently small turn radius, the urban vehicle may even be able to make U-turns on a 2-lane city road without reversing, thus significantly reducing their disturbance to traffic flow. This feature is a requirement for the project vehicle.

Based on road design criteria published by the US Department of Transportation [28], the width of local traffic lanes should be no less than 2.7 m. The narrowest two-way roads should thus be about 5.4 m wide. Adding some contingency, the turn radius of the project vehicle should therefore be small enough such that it fully clears a road 5 m across while performing a U-turn.

2.3.2.2 Rollover Resistance

Rollover resistance can be quantified using a static stability factor (SSF) defined and reported by the NHTSA in its New Car Assessment Program (NCAP) ratings [29]. In essence, the SSF is the ratio of a vehicle’s half-track to the height of its center of gravity.

The higher the ratio, the more resistant the vehicle is to rollover. Though relatively simple, the SSF is versatile because it is strongly correlated to rollover both with and without tripping by obstacles. To give an idea of typical SSF values, Table 5 shows the average SSF of various vehicle types over the past few decades [29].

Table 5 – Trends in average SSF by vehicle type, weighted by vehicle sales data [29]

Year	Passenger cars	SUV	Pickup trucks	Minivans	Full vans
1975	1.09				
1976	1.10				
1977	1.09				
1978	1.38	1.10			
1979	1.38	1.08			
1980	1.36	1.07			
1981	1.37	1.07	1.20		
1982	1.36	1.08	1.20		
1983	1.36	1.07	1.17		
1984	1.36	1.06	1.15		
1985	1.36	1.08	1.18	1.11	1.09
1986	1.36	1.07	1.18	1.11	1.09
1987	1.36	1.07	1.18	1.11	1.09
1988	1.35	1.07	1.17	1.15	1.09
1989	1.36	1.08	1.18	1.15	1.09
1990	1.37	1.07	1.17	1.16	1.09
1991	1.38	1.08	1.18	1.17	1.09
1992	1.39	1.08	1.18	1.17	1.11
1993	1.39	1.09	1.18	1.17	1.11
1994	1.40	1.09	1.18	1.17	1.11
1995	1.41	1.09	1.18	1.19	1.11
1996	1.41	1.09	1.18	1.21	1.11
1997	1.41	1.10	1.18	1.20	1.11
1998	1.42	1.10	1.17	1.22	1.12
1999	1.42	1.11	1.18	1.23	1.12
2000	1.42	1.11	1.18	1.24	1.12
2001	1.42	1.14	1.18	1.24	1.12
2002	1.42	1.15	1.19	1.24	1.12
2003	1.41	1.17	1.18	1.24	1.12

When reporting rollover resistance to consumers, NCAP uses a simplified star rating system shown on Table 6. As the development of CWMs for rollover resistance is one of the main focuses of the project vehicle, the ability to attain a five-star rating should be made a design requirement.

Table 6 – NCAP star rating for rollover resistance [30]

Star rating	Risk of rollover in a crash
★★★★★	<10%
★★★★	10-20%
★★★	20-30%
★★	30-40%
★	>40%

The method of conversion between SSF and the star rating system has changed throughout the years. Prior to 2004, star rating depended on SSF alone, but after 2004, results from dynamic turning tests (namely fishhook manoeuvres) were incorporated as well [29]. Since the project vehicle is still in its early stages of design, only SSF will be accounted for. Dynamic simulations should be performed once the design of wheel modules is sufficiently mature.

The rollover risk of a vehicle is calculated using a logistic regression between SSF and 293,000 recorded crashes in the US that involved rollover [30]. From Figure 8, it can be seen that likelihood of rollover during a crash increases in a roughly exponential relationship with decreasing SSF. To obtain a best fit line for this relationship, the NHTSA applied a number of mathematical manipulations to a basic $\log(SSF)$ curve, with the final result as follows:

$$R = \frac{1}{1 + e^{(2.7546 + 1.1814 \times \ln(SSF - 0.9))}} \quad \textbf{(2.1)}$$

where R is rollover risk. Solving for SSF gives:

$$SSF = e^{\left(\frac{\ln(1/R - 1) - 2.7546}{1.1814}\right)} + 0.9 \quad \textbf{(2.2)}$$

To obtain a 5 star rating, the project vehicle needs to have a rollover risk of less than 10%. Using equation (2.2), the minimum required SSF is calculated to be 1.52. Since vehicle rollover occurs when the net force vector acting on the vehicle center of mass intersects the ground at a point outside the perimeter formed by the tire contact patches, we can further deduce that:

$$SSF = \frac{\frac{1}{2}t}{h} = \frac{ma_{ymax}}{mg} = \frac{a_{ymax}}{g} \tag{2.3}$$

where a_{ymax} is the maximum static lateral acceleration that the vehicle can sustain before it rolls over and g is acceleration due to gravity. An SSF of 1.52 thus corresponds to an a_{ymax} of $1.52g$. Since the rollover resistance of a three-wheeled vehicle is affected by longitudinal acceleration, the specification of $a_{ymax} = 1.52g$ shall correspond to the case of zero longitudinal acceleration.

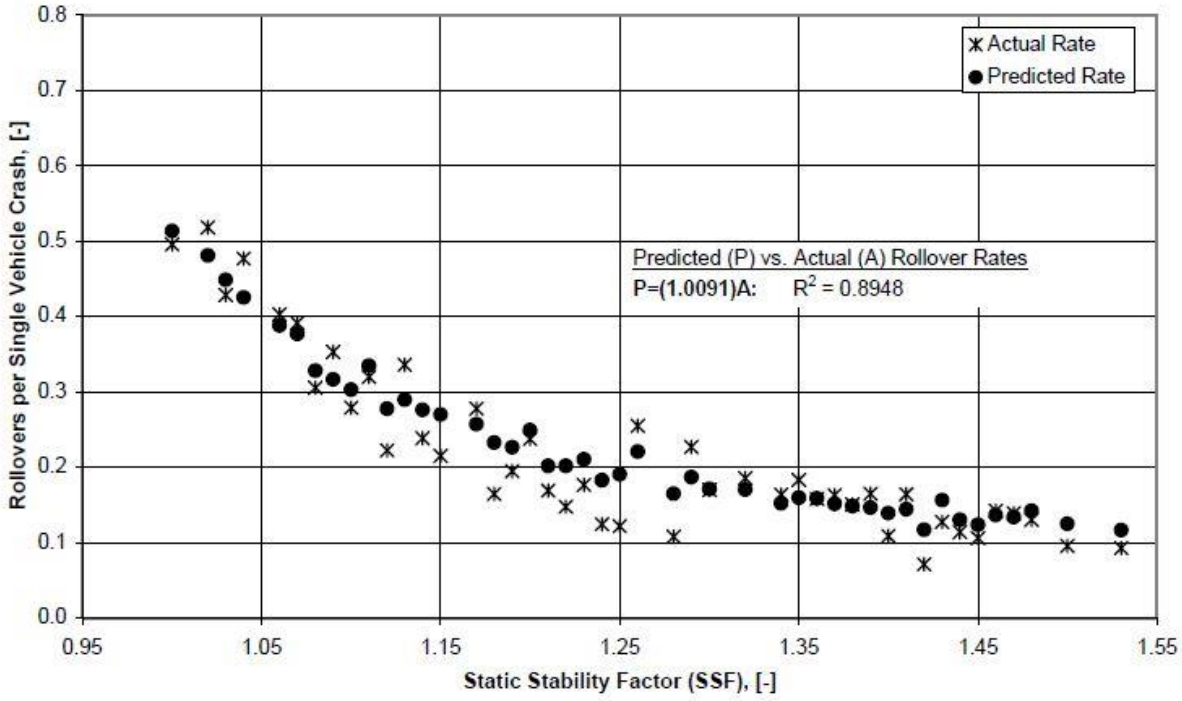

Figure 8 – Relationship between static stability factor and rollover risk [30]

2.3.2.3 Steering Response

Steering response refers to how the vehicle responds to steering inputs at various speeds. Steering response can be categorized into understeer, neutral steer, or oversteer. During cornering, if the steering angle of the wheels is held constant while vehicle speed is increased, an understeer vehicle would veer to the outside of the turn, an oversteer vehicle would veer into the turn, and a neutral vehicle would do neither (Figure 9).

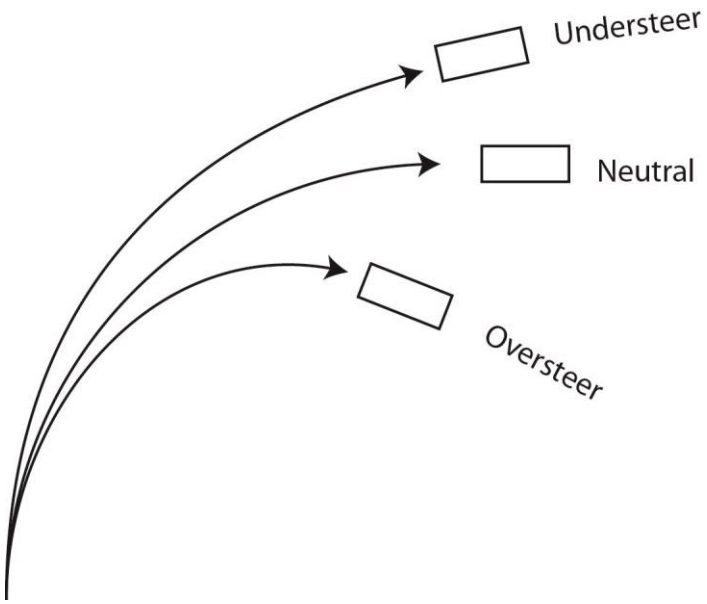

Figure 9 – Behavior of different cars during cornering with increasing speed

For normal passenger cars, understeer behavior is desirable for safety. All vehicles tend to lose directional control when cornering at excessive speed. In such an event, an understeer vehicle would tend to continue along a straight line, and the driver may regain control by simply slowing down. However, an oversteer vehicle would turn violently, resulting in a spinout that is virtually impossible to recover from. Although neutral steer vehicles are at a lesser risk of spinouts compared to oversteer vehicles, they are still too difficult to handle for typical drivers.

Another factor that makes oversteer vehicles especially unsafe is that since the turn radius of an oversteer vehicle decreases with speed, there is a certain critical speed v_{crit} where turn radius tends to zero [31]. At such a speed, the steering response of the vehicle

becomes so sensitive that even minimal steering inputs would cause the vehicle to spin out of control. Furthermore, v_{crit} decreases with increasing oversteering characteristic, which means strongly oversteer vehicles would tend to lose control even at low speeds.

Steering characteristic is controlled by two factors: the front/rear weight distribution and the balance in total cornering stiffness between the front and rear axles. The cornering stiffness of a tire is the amount of lateral force it generates per unit slip angle (assuming small steer angles). For a four-wheel vehicle with a weight distribution of exactly 50/50 (i.e. center of gravity is at center of wheelbase) and front and rear tires of equal cornering stiffness, steering characteristic is neutral (Figure 10 a). If the CG is shifted rearward, the moment arms of the front tires acting on the CG become longer than that of the rear tires, so there is an overall moment that tends to turn the car further into the corner (Figure 10 b). This moment increases if the force on both tires is increased (e.g. if the vehicle corners faster and/or sharper), resulting in behavior that is characteristic of oversteering. If the CG is shifted forward instead of rearward, the mechanism is reversed and the vehicle becomes understeer (Figure 10 c). Understeer behavior can also be obtained if weight distribution remains at 50/50 but tires of high cornering stiffness are installed on the rear (Figure 10 d).

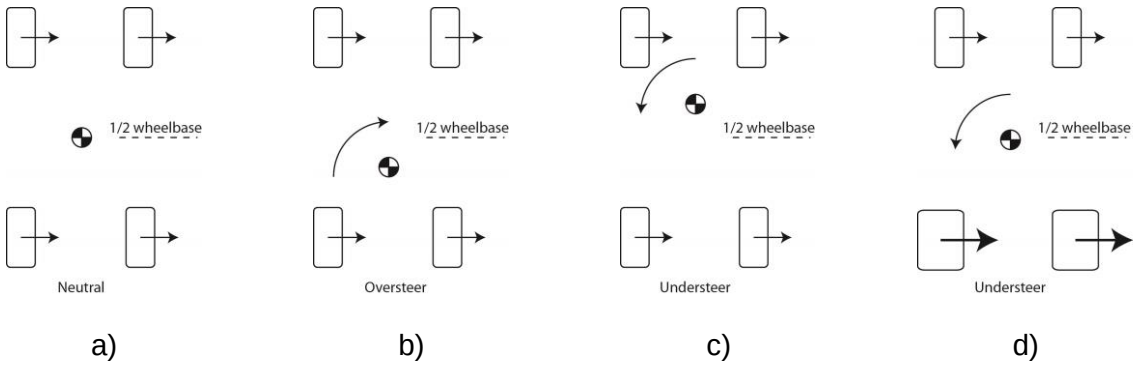

Figure 10 – Steering responses of four-wheel vehicles making a right turn

In the case of a three-wheeled vehicle with uniform tires, neutral steer is obtained if the center of gravity is located at 1/3 of wheelbase rearward of the front axle (Figure 11 a), since the front axle has twice the total cornering stiffness of the rear axle. As with four-wheel vehicles, oversteering behavior results if the center of gravity is shifted rearward from the neutral point (Figure 11 b). If maintaining a forward-biased weight distribution is difficult, steering characteristic can be shifted towards the understeer end of the spectrum by

increasing the cornering stiffness of the rear tire (Figure 11 c). If all the wheels of the vehicle are steerable, as is in the case of the project vehicle, there is yet another possibility: the rear wheel can be steered into the corner to generate additional cornering force, thus shifting steering response towards understeer (Figure 11 d).

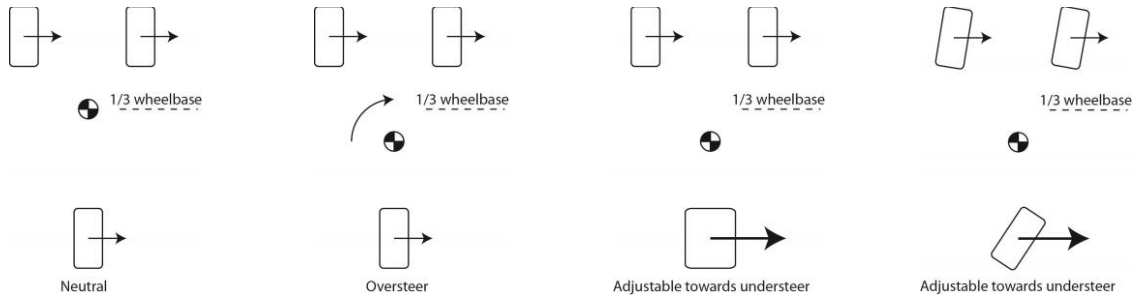

Figure 11 – Steering responses of three-wheel vehicles making a right turn

One difficulty with the all-wheels-independently-steerable solution is that as lateral acceleration increases, steering angles would need to be controlled with increasing accuracy and responsiveness to avoid oversteer. If the performance limits of the drive-by-wire system are known, it would be possible to specify a CG location and maximum lateral acceleration such that the limits are never exceeded. Since such data is not yet available, a simpler requirement for steering response would be that assuming the vehicle is front-wheel-steered, the longitudinal position of the CG must be far enough forward such that if oversteer behavior is unavoidable, the critical speed of the vehicle must be well above its maximum speed. Though grossly simplified, this specification is still useful as a worst-case-scenario baseline, since the ability to steer the rear wheel on an all-wheel steer-by-wire makes it invariably more stable than a front-wheel steering system.

2.3.3 Crashworthiness

Legal requirements for road vehicle crashworthiness in the US and Canada are specified in the FMVSS and CMVSS, respectively. These regulations represent the minimum requirements that a production vehicle must meet before it can drive on public roads. Besides satisfying these minimum requirements, production vehicles are often given more stringent tests under NCAP and Insurance Institute for Highway Safety (IIHS). NCAP grades

vehicles using a star rating system based on how well they protect their occupants, with five stars being the highest score. Considering that part of the vehicle project involves development of foam crash structure technology, it is reasonable to aim for a five star rating under all NCAP crash tests so as to demonstrate the value of this technology.

There are three crash tests under US NCAP: frontal impact, side impact, and side pole impact [32] (Figure 12). For simplicity at this early stage of design, only the front and side impact will be considered.

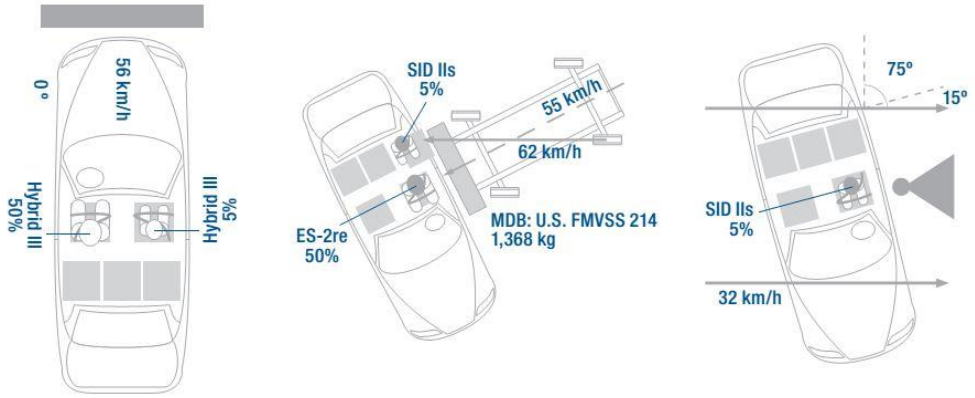

Figure 12 – Crash tests under US NCAP [32]

In the frontal impact test, the vehicle is driven into a barrier at 56 km/h, and impact forces are measured on various parts of the crash test dummy. The measured impact forces are used to estimate risk of occupant injury, which is then translated into a star rating for ease of consumer understanding. Among the many variables assessed, two variables are found to correlate well with the star rating: chest acceleration and head injury criterion (HIC) [33]. Assuming that the occupant is firmly secured to the vehicle using a seatbelt, chest acceleration upon impact should be approximately equal to acceleration of the vehicle cabin, which can be estimated even at the earliest stages of design. In reality, airbags and seat belt slack can be used to further reduce chest acceleration. Estimation of HIC is more complex as it depends on the design of more detailed components such as airbags and steering wheels. At this stage of design, frontal crash safety will be specified only in terms of vehicle cabin acceleration upon impact. From Figure 13, it can be seen that in order to obtain a five-star rating, the cabin acceleration should not exceed 46 g.

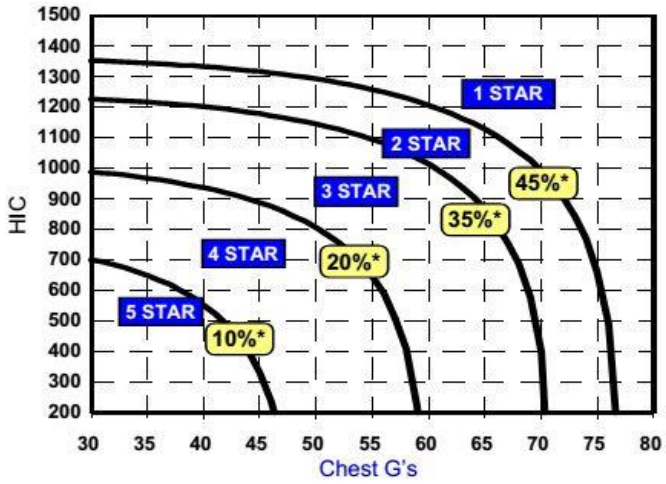

Figure 13 – Determination of NCAP frontal crash rating [33]

In US NACP side crash tests, a moving deformable barrier weighing 1370 kg is driven into the side of a stationary test vehicle at an angle of 27 degrees with an initial speed of 62 km/h (Figure 12). In contrast to the frontal crash test, there should be little deformation of the vehicle structure. Instead, occupant impact forces are reduced by a soft region on the inner side of the door, which contains components like side airbags and door trim panels. Crash safety is measured in terms of the Thoracic Trauma Index (TTI), which is defined as the average of the peak accelerations in the rib and lower spine [34]. As a simplification, TTI will be assumed to be roughly equal to the average acceleration of the occupant, which is easier to calculate. To achieve a five-star rating for side crash, average occupant acceleration should not exceed 57 g (Table 7).

Table 7 – Determination of NCAP side crash rating [35]

Star rating	Risk of injury	TTI (g)
★★★★★	<5 %	TTI ≤ 57
★★★★	6-10%	57 < TTI ≤ 72
★★★	11-20%	72 < TTI ≤ 91
★★	21-25%	91 < TTI ≤ 98
★	>26%	TTI > 98

2.4 Summary

The form and performance specifications generated in this chapter are summarized on Table 8 and Table 9, respectively. In the next chapter, calculation methodologies will be developed to drive the design process with adherence to these specifications.

Table 8 – Summary of form specifications

Number of wheels	3
Propulsion	Three electric motors
Steering actuation	Electrical
Primary energy storage type	Lithium ion batteries
Seating arrangement	Two passengers side-by-side
Occupant space	Develop according to SAE standards J1052 and J4004
Length	As small as possible without compromising other requirements
Width	As small as possible without compromising other requirements; width with all doors open must not exceed 2500 mm
Height	As small as possible without compromising other requirements
Ground clearance	> 160 mm
Front bumper clearance	> 203 mm
Rear bumper clearance	> 203 mm
Approach angle	> 16 degrees
Departure angle	> 13 degrees
Ramp-over angle	> 12 degrees

Table 9 – Summary of performance specifications

Maximum range	> 110 km under New York City Cycle
Speed-acceleration profile	See Figure 4
Gradeability at 50 km/h	12%
Maximum gradeability	20%
Minimum turn radius	Sufficient clearance for U-turn on 5.4 m wide lane without reversing
Overturning threshold	Obtain NCAP five-star rating. Interim requirement: with wheels at full camber, achieve SSF of 1.52 g assuming no longitudinal acceleration
Steering response	Steer-by-wire system must be able to generate understeer response through entire vehicle speed range. Interim requirement: assuming front-wheel-steer, if oversteer response is unavoidable, critical velocity must be significantly above maximum speed
Front impact safety	Obtain NCAP five-star rating. Interim requirement: peak cabin acceleration must not exceed 46 g
Side impact safety	Obtain NCAP five-star rating. Interim requirement: average occupant acceleration must not exceed 57 g

Chapter 3 Tools for Conceptual and Embodiment Design

3.1 Introduction

In this chapter, tools will be developed to aid in conceptual and embodiment design. These tools take the form of calculation approaches and simulation models that can be used to determine the required size, weight, or characteristics of a vehicle component. A list of tools developed in this chapter as well as their method of implementation, outputs, and application is shown on Table 10. Since the design of the vehicle is still in its early stages, the tools developed here are only sufficiently accurate for order-of-magnitude estimations. As the design progresses and more information become available, the tools should grow in sophistication accordingly so as to provide more accurate results.

Table 10 – Summary of tools developed and their applications

Model	Implementation	Outputs	Application
Occupant packaging model	CAD model		Size and weight of occupants
Crumple zone model	Spreadsheet		Size of crumple zones
Acceleration model	Spreadsheet	• Acceleration • Maximum speed • Gradeability	Motor sizing
Drive cycle model	Spreadsheet	• Economy • Range	Battery sizing
Rollover threshold model	Spreadsheet	Rollover threshold	Allowable CG location
Steering response model	Spreadsheet	Steering response	Allowable CG location

The role of these tools in the overall design process is shown on Figure 14. In the case of both conceptual and embodiment design, major vehicle components must be sized before a viable vehicle package can be produced. The occupant packaging model, crumple zone model, and drive cycle model are used to size the occupants, crumple zones, and batteries,

respectively. Once these components are sized, they are arranged in a vehicle package, and their positions and weights determine the CG location and weight of the vehicle. The rollover threshold model and steering response model help ensure that the vehicle package leads to a dynamically feasible vehicle. Each models will be discussed in more detail below.

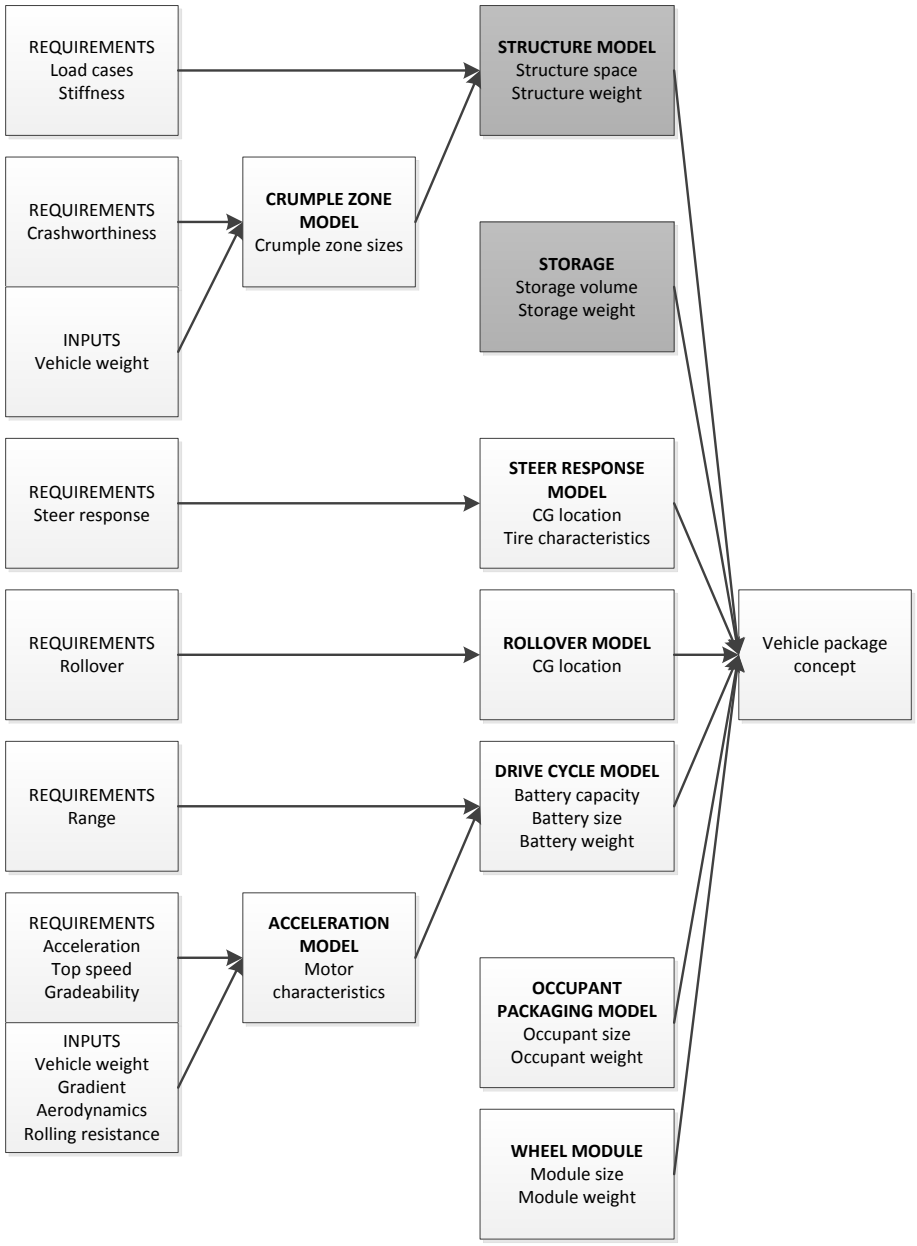

Figure 14 – Overview of the design approach; items in dark boxes are not considered in this thesis

3.2 Occupant Packaging Model

An occupant packaging model was built based on SAE standards J4004 and J1052 [5] [4]. The model ensures that there is sufficient interior space in the project vehicle to accommodate two occupants with body dimensions of the 95th percentile US male. Once fully defined, there will be only three degrees of freedom for adjusting occupant posture – the seat height and longitudinal/vertical location of the steering wheel center. All other dimensions are calculated based on these to produce a posture for best comfort. The occupant packaging model developed in this thesis includes the following elements:

- **Legs (section 3.2.1)**: legs are positioned for seating comfort. A mathematical function is used to calculate how far forward the legs extend with a given seat height. This function is based on studies that examine natural leg positions of seated individuals.
- **Feet (section 3.2.1)**: once natural leg position is calculated, the angle of the driver's feet can be calculated using another mathematical function. Feet angle is useful not only for determining the forward extent of the driver, but also the design of foot pedals later on.
- **Seat track line (section 3.2.2)**: this is a line representing the extent of possible forward and rearward adjustment of the seat. The length of this line is determined based on the percent of body sizes to be accommodated by the seat. A longer line will allow the seat to accommodate a greater variety of body sizes. In terms of occupant packaging, the seat track line is useful for defining the rearmost extent of the seat, as the position of the driver's feet stay fixed as the seat is adjusted. In addition to horizontal adjustment, some seats can be adjusted vertically as well, in which case a seat adjustment zone rather than a seat track line is defined. At this early stage of design, however, only a seat track line will be defined.
- **Head clearance envelope (section 3.2.3)**: a semi-ellipsoid surface representing area reserved for head movement. This envelope is created based on SAE standard J1052.

A few additional elements related to occupant packaging are defined in the SAE handbook but will not be considered in detail at this early stage of design. The elements are listed as follows:

- **Eyellipses**: ellipsoids representing the regions where the driver's eyes are most likely to be located. These will become important when vision studies are performed later on during the design of windows and mirrors.
- **Reach envelopes**: surfaces representing the minimum or maximum distance that a restrained occupant can reach. These will become important during the design of user interfaces.

The following sections will discuss in detail how each occupant element is defined.

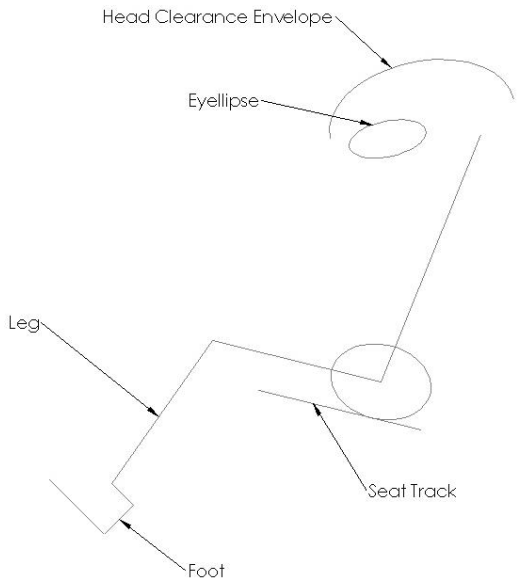

Figure 15 – 2D occupant package model

3.2.1 Legs and Feet

The positions of legs and feet are calculated using mathematical functions to ensure best comfort. Figure 16 depicts the legs and feet of the occupant with SAE-defined reference points and dimensions shown. The reference points and dimensions are defined as follows:

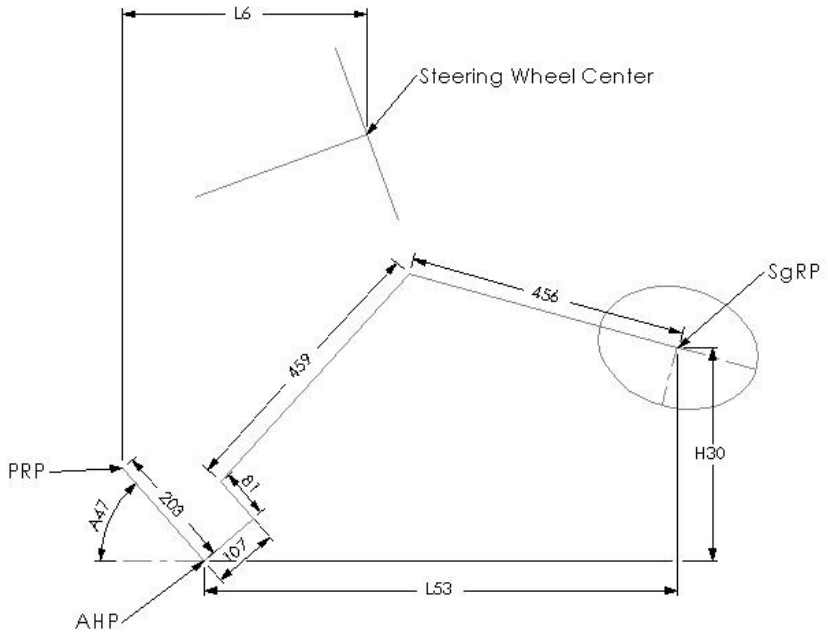

Figure 16 – Occupant legs and feet with important dimensions and reference points

- **Accelerator Heel Point (AHP)** represents the location of the driver's heels.
- **Pedal Reference Point (PRP)** is the point of contact between the driver's foot and a pedal.
- **H-Point** is the location of the driver's hip joint. The H-point is free to travel along a seat adjustment track or within a seat adjustment zone.
- **Seating Reference Point (SgRP)** represents a particular location of the H-point defined for occupant packaging purposes. Usually, the H-point location of a naturally seated 95th percentile US male is used as the SgRP. The position of the SgRP relative to the AHP is defined using the dimensions L53 and H30.
- **H30** is the vertical distance between AHP and SgRP. This is often an independent variable from which other variables like A47 and L53 are calculated.
- **A47** is the angle of the driver's feet from horizontal, measured at the bottom of his shoe. The formula for A47 is:

$$A47 = 77 - 0.08(H30) \quad \textbf{(3.1)}$$

- **L53** is the horizontal distance between AHP and SgRP. The formula for L53 is:

$$L53 = [913.7 + 0.672316(H30) - 0.0019553(H30)^2] - 203 \times \cos(A47) \quad \textbf{(3.2)}$$

- **L6** is the horizontal distance between the PRP and the center of the steering wheel. Although the steering wheel is not designed in this project, L6 is required for calculating the seat track and head clearance envelope.

3.2.2 Seat Track

Seat track recommendations from SAE standard J4004 are specified in terms of a reference point located at distance X_{ref} rearward of the pedal reference point and a seat track that extends fore and aft of this reference point. For vehicles without a clutch pedal, the reference point is located at:

$$X_{ref} = 718 - 0.24(H30) + 0.41(L6) \quad \textbf{(3.3)}$$

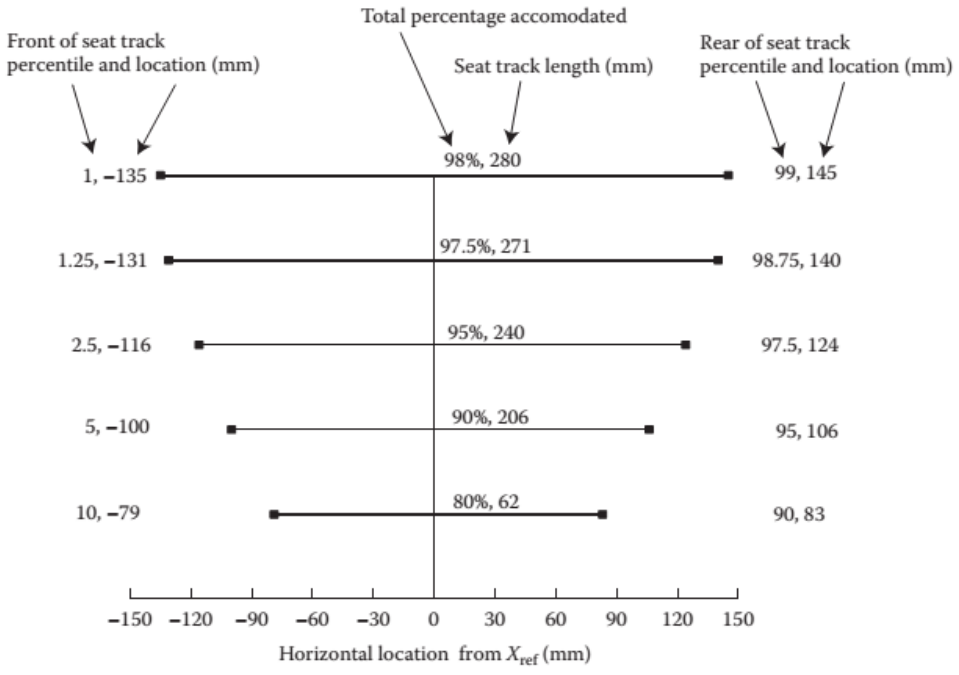

Figure 17 – Recommended seat track length relative to reference point [4]

The length of the seat track forward and aft of the reference point is determined based on the percent of body sizes seat is to accommodate. For example, to accommodate 95% of all body sizes, the seat track line should extend 116 mm forward and 124 mm rearward from the reference point (Figure 17). The seat track line is at a 10 degree upward angle centered at the reference point because the front end of the seat track is used by shorter drivers, who need to sit higher to see the road.

3.2.3 Head Clearance Envelope

The head clearance envelope is defined in SAE standard J1052 as an ellipsoidal dome surface. Four envelope sizes are given in J1052, one for each combination of percent driver population covered (95% or 99%) and seat track length (above or below 133 mm). The center of the head clearance envelope is placed at a fixed coordinate relative to the SgRP.

3.2.4 Three-Dimensional Model and Center of Mass

The SAE occupant packaging method used in the previous sections is in only two dimensions. Two unknown dimensions are needed to extend the model to three dimensions: the shoulder and hip widths of the 95th percentile US male. These are given by Bhise [4] as 620 mm and 412 mm, respectively. Using the posture calculated in the previous sections as a “skeleton,” a full 3D CAD model of the occupant was produced (Figure 18).

Aside from dimensions, the occupant’s center of mass is also of interest when it comes to evaluating vehicle dynamics. The center of mass of a seated individual was measured by Swearingen [36] to be approximately 8.75 inches (222 mm) above the seat surface and 7.5 inches (190 mm) from the seat back. So long as the occupant remains in a seated position, the movement of his CG due to changes in arm or leg posture is within a few inches, which is negligible for the purpose of evaluating vehicle dynamics.

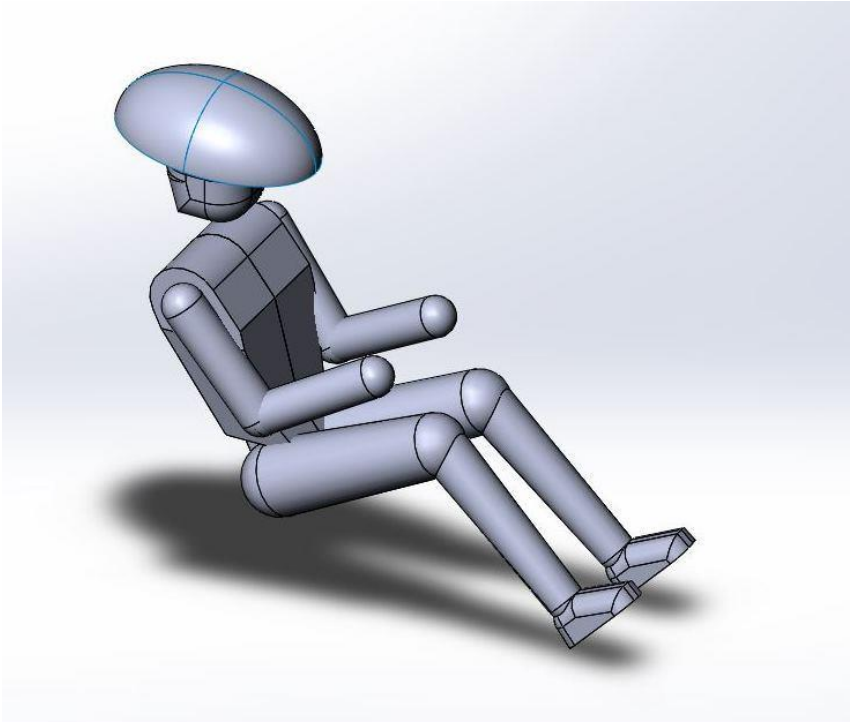

Figure 18 – 3D occupant model

3.3 Crumple Zones

A crumple zone sizing model developed by Malen [34] was used to approximate crumple space requirements for front, side and rear crash scenarios.

3.3.1 Front Crash Structure

The front crumple zone can be approximately sized if impact speed, cabin acceleration target, and frontal structure crush efficiency are known. For a US-NCAP test, the frontal impact speed is 56 km/h [33]. Cabin acceleration and structure crush efficiency are assigned as targets to be used for crash structure design.

Structure crush efficiency is a measure of how well a structure is able to maintain an even cabin acceleration as it deforms. Poor crush efficiency can result if the crash structure lacks homogeneity in terms of deformability, as often is the case when rigid components like the engine are mixed with softer structural supports. In the case of the project vehicle, metal foam will be incorporated in the crash structure to greatly improve crash efficiency. Since

little is currently known about the crash structure, a crash efficiency of 90% will be assumed achievable.

To size the front crumple zone, we start by equating the kinetic energy of the vehicle with the energy dissipated by the crush structure as it crumples:

$$\frac{1}{2}mv_0^2 = F_{avg}\Delta \tag{3.4}$$

where m is the mass of the vehicle, v_0 is initial vehicle speed, F_{avg} is the average force generated by the crash structure to slow down the vehicle, and Δ is the length of the crumple zone. In term of crash safety, it is not the average force, but the maximum force that is of concern. The maximum force is related to average force by

$$F_{avg} = \eta F_{max} \tag{3.5}$$

where η is the crush efficiency factor. Substituting F_{max} into equation (3.4) and replacing F_{max}/m with a_{max} gives:

$$\Delta = \frac{v_0^2}{2\eta a_{max}} \tag{3.6}$$

3.3.2 Side Crash Structure

Side crash structures can be sized given vehicle mass, rigidity of the outer door structure, and an occupant acceleration target. A side crash structure differs from a front crash structure in that the reduction in occupant acceleration is achieved primarily through a region of soft material on the inner side of the door rather than deformation of the vehicle structure. Sizing of the door involves sizing of the rigid outer door shell, the soft region, and the gap between the occupant and soft region. Before proceeding with crash structure sizing calculations, it is useful to first examine the kinematic details of a side crash.

Table 11 lists the sub-events that occur during a side crash. At time t_0, the barrier and vehicle make first contact. The barrier slows down while the vehicle speeds up until they reach a common speed the end of collision, t_2. If there is a gap between the interior door panel and the occupant, the occupant will remain stationary between t_0 and t_1 as the door

panel closes the gap. At time t_1, the gap fully closes and the interior door panel makes contact with the occupant, accelerating him until they reach the same speed at time t_f. The average acceleration experienced by the occupant between t_1 and t_f is assume to be roughly equal to TTI. A major simplifying assumption for the overall side crash is that all accelerations are constant. Figure 19 shows that as a rough order of magnitude calculation, this assumption is reasonable.

Table 11 – List of events that occur during a side crash

Time	Barrier	Vehicle	Occupant
t_0	Contact with vehicle, starts decelerating	Contact with barrier, starts accelerating	Stationary
t_1	Continue decelerating	Continue accelerating	Contact with door, starts accelerating
t_f	Continue decelerating	Continue accelerating	End of collision with door, match barrier speed
t_2	End of collision, speeds converge	End of collision, speeds converge	End of collision, speeds converge

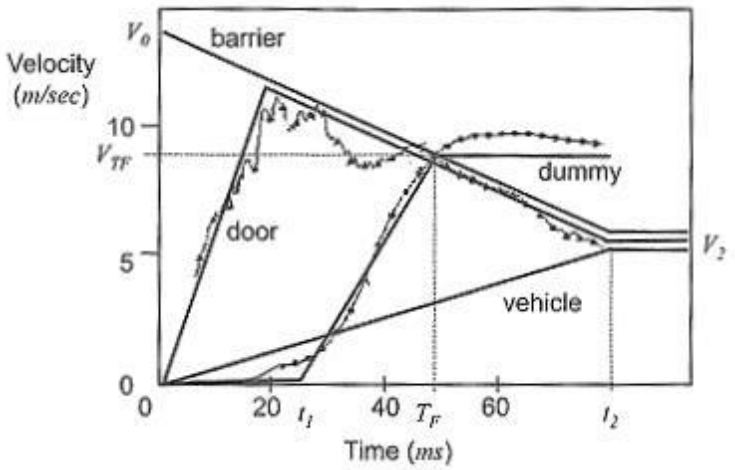

Figure 19 – Time history of a side crash with linear approximations [34]

Proceeding with crash structure sizing calculations, the momentums of the barrier and vehicle are first equated to find the final velocity at the end of the impact:

$$m_1 v_0 = (m_1 + m_2) v_2$$

$$v_2 = \frac{m_1}{m_1 + m_2} v_0 \quad \textbf{(3.7)}$$

where m_1 is the mass of the barrier, m_2 is the mass of the vehicle, v_0 is the component of the initial velocity of the barrier perpendicular to the vehicle door (for an NCAP test, this is about $61.6 \times \cos 23 = 56.7\ km/h$), and v_2 is the final speed of the barrier and vehicle. Next, the rate at which the barrier and vehicle accelerate towards the final speed is determined as follows:

$$a_1 = -F_2/m_1 \quad \textbf{(3.8)}$$

$$a_2 = F_2/m_2 \quad \textbf{(3.9)}$$

where a_1 is the acceleration of the barrier, a_2 is the acceleration of the vehicle, and F_2 is the force between the barrier and vehicle. F_2 depends on the rigidity of the door; a more rigid door will generate a higher F_2. High F_2 is desirable because it would slow down the barrier more quickly and reduce the speed at which the barrier and door collide with the occupant. However, F_2 cannot exceed 290,000 N due to the design of the barrier [34]. With acceleration known, the collision end time t_2 can be calculated by:

$$t_2 = \frac{v_2}{a_2} \quad \textbf{(3.10)}$$

The total crush of the vehicle can be calculated by taking the difference between distance travelled by the barrier and vehicle at t_2:

$$crush = \frac{1}{2} v_0 t_2 \quad \textbf{(3.11)}$$

This crush distance is also the required thickness of the side crumple zone. Next, the time at which the occupant strikes the door trim panel is calculated by first equating vehicle travel with the gap between the occupant and the door:

$$\frac{1}{2}[v_0 + (v_0 + a_1 t_1)]t_1 = \Delta_0 \quad \textbf{(3.12)}$$

where t_1 is the time of occupant contact with the door trim panel, and Δ_0 is the initial gap between the occupant and the trim panel. After assigning a value for Δ_0, t_1 can be solved for using the quadratic formula as follows:

$$t_1 = \frac{-\frac{2v_0}{a_1} \pm \sqrt{\left(\frac{2v_0}{a_1}\right)^2 + 4\left(\frac{2\Delta_0}{a_1}\right)}}{2} \quad \textbf{(3.13)}$$

The remaining task is to determine when the occupant-door collision ends, and at what speed. To calculate these, the door interior crush zone Δ needs to be specified. By equating Δ with the relative distance travelled between the occupant and the door, the following equations are obtained:

$$\frac{1}{2}(t_f - t_1)v_1 = \Delta$$

$$v_1 = v_0 + a_1 t_1$$

$$t_f = \frac{2\Delta}{v_0 + a_1 t_1} + t_1 \quad \textbf{(3.14)}$$

where v_1 is the speed of the door and barrier upon contact with the occupant, and t_f is the time when the occupant reaches the same speed as the door/barrier. The speed at t_f can be calculated as follows:

$$v_{tf} = v_0 + a_1 t_f \quad \textbf{(3.15)}$$

Average acceleration of the occupant can then be calculated as follows:

$$a_{occ} = \frac{v_{tf}}{t_f - t_1} \quad \textbf{(3.16)}$$

A summary of calculations describing a side crash is provided on Table 12. An example plot of this data is shown on Figure 21 a).

The effects of adjusting vehicle mass, door rigidity, and door trim dimensions are shown on Figure 21 a, b and c, respectively. With an increase in vehicle mass (Figure 21 a), the final speed of the vehicle and barrier at the end of collision is decreased, but this does not affect the acceleration of the occupant, which is assumed not to be restrained to the vehicle. The speed v_1 at which the door collides with the occupant remains the same. With increased door rigidity (Figure 21 b), the acceleration force between barrier and vehicle is

increased such that they reach the final velocity sooner. This has the effect of slowing down the barrier and door before it strikes the occupant, thus lowering occupant acceleration. By reducing the occupant-door gap Δ_0 and increasing the trim panel crush space Δ of the door trim panel (Figure 21 c), occupant acceleration starts sooner and ends later, resulting in reduced overall acceleration. If the trim panel is thick enough, the barrier-vehicle collision ends before the occupant reaches maximum velocity (Figure 21 d).

Table 12 – Summary of calculations describing a side crash

Time	Barrier	Vehicle	Occupant
$t_0 = 0$	v_0	0	0
$t_1 = \dfrac{-\frac{2v_0}{a_1} \pm \sqrt{\left(\frac{2v_0}{a_1}\right)^2 + 4\left(\frac{2\Delta_0}{a_1}\right)}}{2}$	$v_1 = v_0 + a_1 t_1$	$a_2 t_1$	0
$t_f = \dfrac{2\Delta}{v_0 + a_1 t_1} + t_1$	$v_0 + a_1 t_f$	$a_2 t_f$	$v_0 + a_1 t_f$
$t_2 = \dfrac{v_2}{a_2}$	$v_2 = \dfrac{m_1}{m_1 + m_2} v_0$		

Note: calculations assume $t_f < t_2$

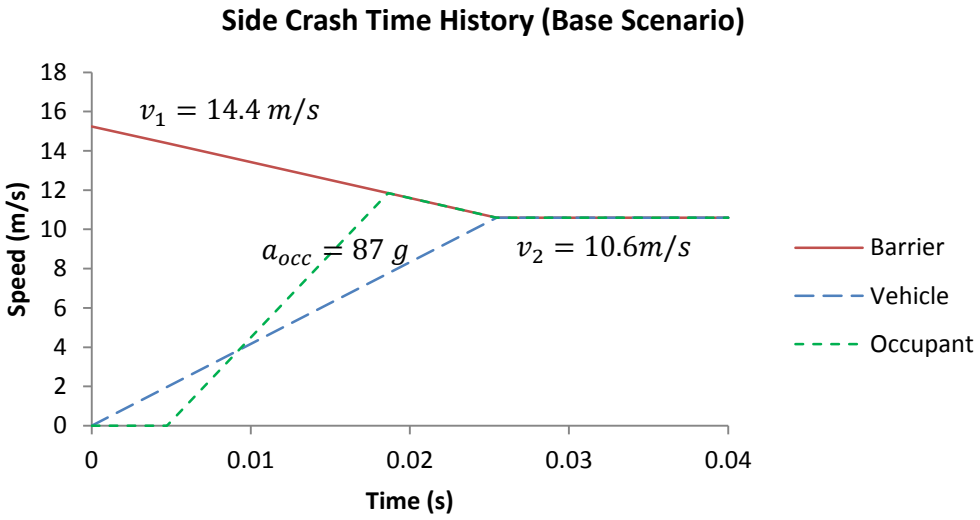

Figure 20 – Linearly approximated time history of a side crash

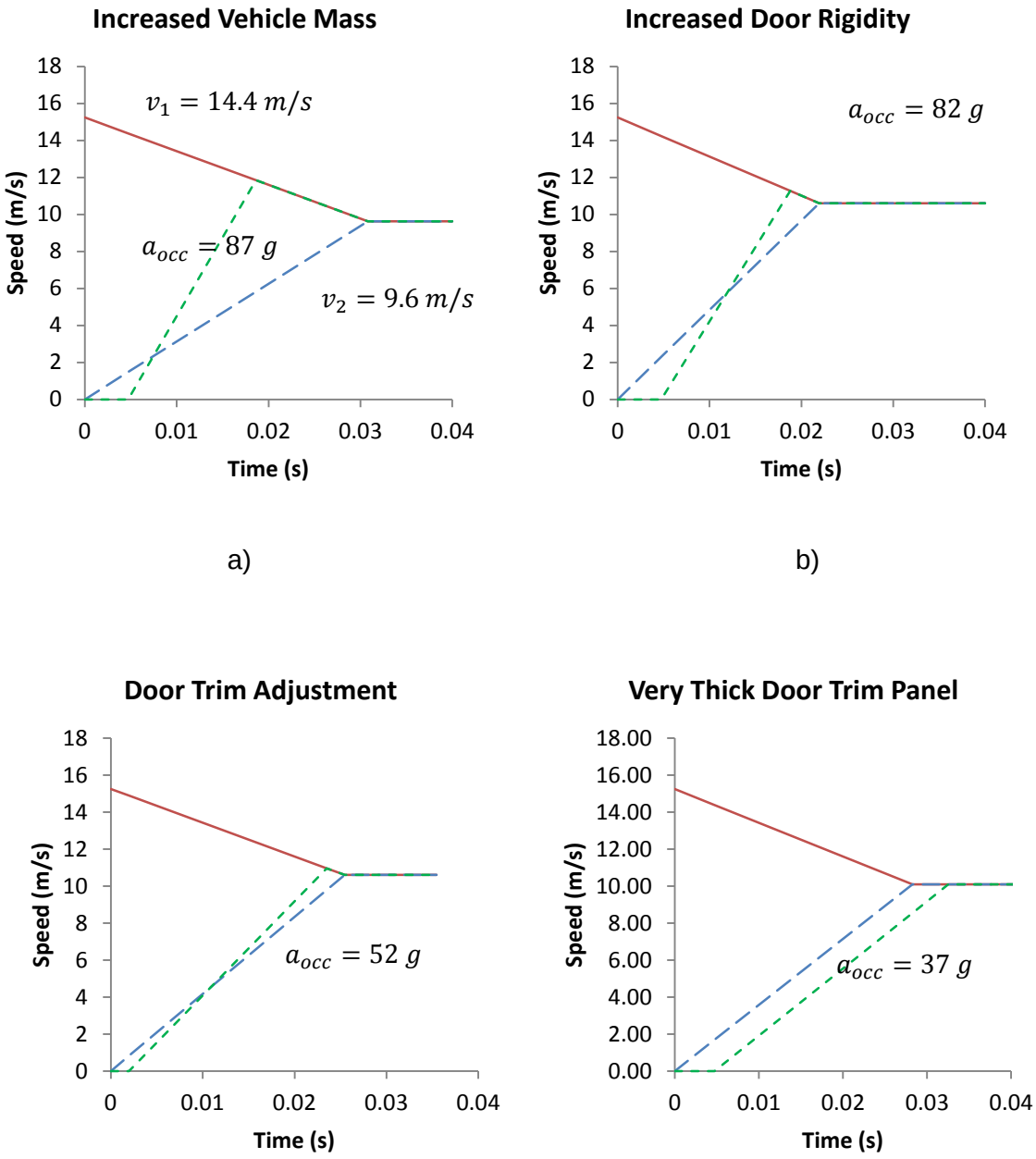

Figure 21 – Linear approximations of side crash time history showing the impact of various parameters on crash dynamics

The final task in this section is to size the vehicle side crash structure to meet safety requirements. The side crash structure is idealized as a rectangular box located outboard of the passenger cabin (Figure 22). The thickness of this box is taken to be the sum of Δ and Δ_0 plus an additional 50% to account for the rigid door structure and the non-crushable portion of the door trim panel. To prevent the barrier from intruding into the passenger cabin, the thickness of the side crash structure must also exceed the crush depth of the vehicle (equation (3.11). Using equations introduced in this section, the crush depth of the vehicle chassis from side impact was found to be 0.19 m if it is sufficiently rigid to achieve 280,000 N of resistance (maximum allowed resistance is 290,000 N). With a door trim thickness of 0.16 m and an occupant-door gap of 0.02 m, an average occupant acceleration of 50.6 g can be achieved, which is below the 57 g required for a 5-star NCAP rating. The total required thickness of the side crash structure is thus 0.27 m.

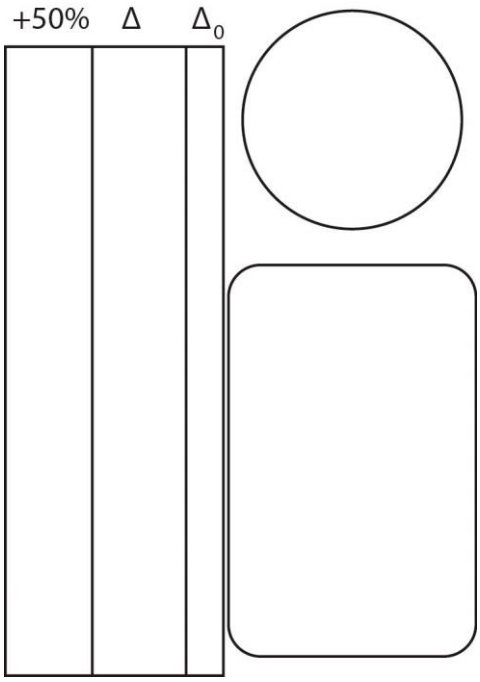

Figure 22 – Idealized side crash structure

3.4 Powertrain

Design of the powertrain involves sizing of the motors and batteries. Two numerical models were developed to simulate powertrain performance: an acceleration model and a drive cycle model. The acceleration model generates an acceleration curve based on road gradient and can be used to evaluate acceleration, top speed, maximum grade at which vehicle can maintain a certain speed, and maximum gradability before stall. The drive cycle model is used for evaluating energy consumption and range given the available battery capacity. The models will be described in more detail in the following sections.

3.4.1 Acceleration Model

The acceleration model is a time-step based numerical model. At each time step, the current speed of the vehicle is used to calculate motor torque and aerodynamic resistance. These, along with gravitational and rolling resistances, are used to calculate acceleration and the speed of the vehicle at the next time step. The sections below will discuss how each force is calculated.

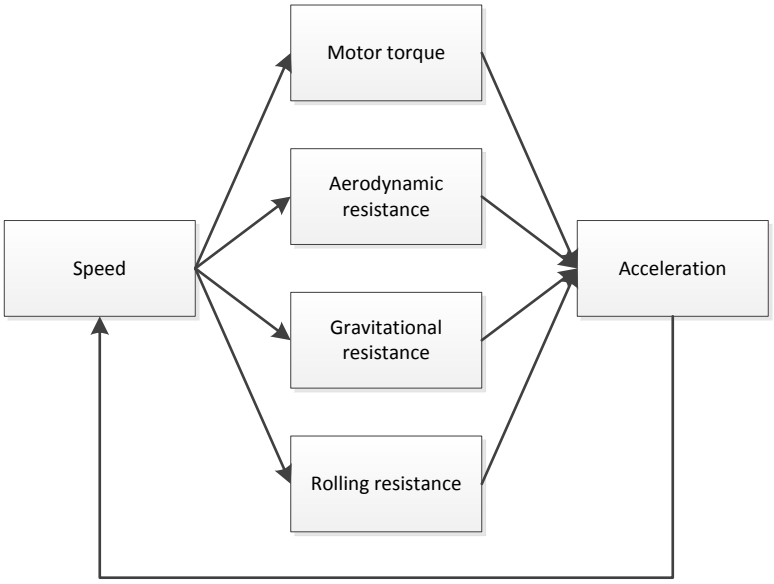

Figure 23 – Overview of the acceleration model

3.4.1.1 Motor Torque

The torque curve of a motor depends on its construction, but most motor torque curves can be approximated with a linear model [37], shown in Figure 24. In the simplified model, there is a range of rotational speeds between zero and rated speed, ω_{rated}, where the available torque is constant at a the rated torque τ_{rated} of the motor. At speeds higher than ω_{rated}, available torque decreases linearly to zero at maximum motor speed ω_{max}. The formula for torque at speeds above ω_{rated} is:

$$\tau = \tau_{rated} - \tau_{rated}\frac{\omega - \omega_{rated}}{\omega_{max} - \omega_{rated}} \quad \textbf{(3.17)}$$

The total acceleration force produced by the motors is simply:

$$F_{mot} = \frac{n\tau}{r_w} \quad \textbf{(3.18)}$$

where r_w is the radius of each wheel and n is the number of motors. As a simplification, the interaction between the tire and the road is not modeled and actual torque delivered to the road is assumed to be equal to torque developed by the motor.

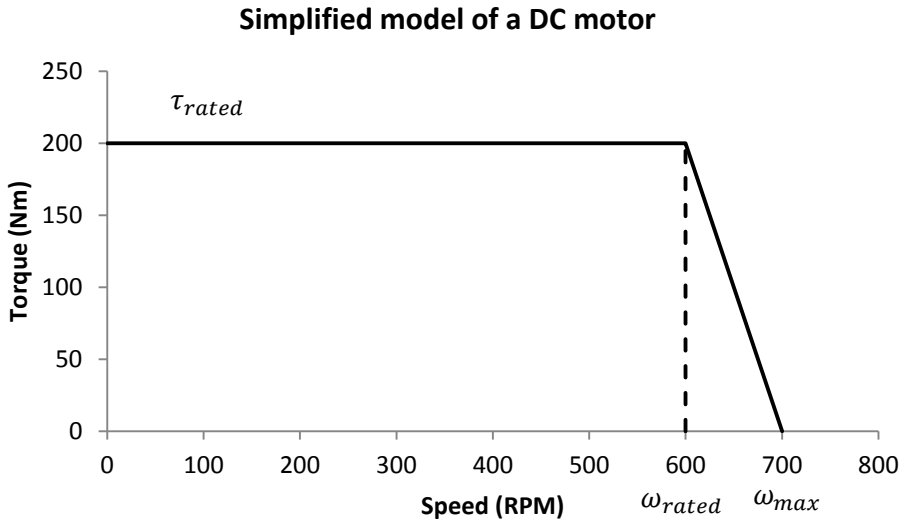

Figure 24 – Simplified torque cruve of a DC motor

3.4.1.2 Aerodynamic and Gravitational Resistance

Aerodynamic resistance force can be calculated using the drag formula:

$$F_{drag} = \frac{1}{2}\rho v^2 C_d A \quad \textbf{(3.19)}$$

where F_{drag} is aerodynamic drag force, ρ is air density, v is vehicle speed, C_d is vehicle drag coefficient, and A is a reference area (commonly the frontal area) on the vehicle.

To check compliance of gradability requirements, the vehicle can be simulated accelerating up a hill. In this case, gravitational force can be broken down into two components:

$$F_{grav} = mg \sin\theta \quad \textbf{(3.20)}$$

$$W = mg \cos\theta \quad \textbf{(3.21)}$$

where F_{grav} and W are the components of gravitational force parallel and perpendicular to the road, respectively, g is acceleration due to gravity, and θ is the angle of the gradient from horizontal. F_{grav} acts directly on the vehicle, pulling it downhill, while W affects the rolling resistance of the tires. In the model, a constant road gradient is used.

3.4.1.3 Rolling Resistance

Although little is currently known about the characteristics of the tires, rough calculations can nevertheless be performed to estimate its rolling resistance. Since tire behavior is difficult to predict from theory, parameters such as rolling resistance would ultimately have to be obtained through tire testing.

Currently the only information available about the tires is their dimensions and the possibility that they may be non-pneumatic solid rubber tires. The tires measure 300 mm in unloaded outer radius, 50 mm in thickness, and 150 mm in width. If vertical loading and material properties of the rubber used is known, there is sufficient information for a rough estimation of rolling resistance.

A method for performing the calculation was proposed by Evans [38] in his 1953 paper. Despite its age, it is still one of the only papers available that presents a general approach for calculating the rolling resistance of solid rubber tires, whereas more recent papers tend to focus on specific designs such as wheelchair tires [39] and tires with solid spokes [40].

The formula for rolling resistance developed by Evans is derived from earlier work on estimation of stresses on cylindrical bodies. The final form of the derivation is:

$$F_{rr} \cong \frac{h}{4.4}\left(\frac{W^4 t}{E s r_w^2}\right)^{\frac{1}{3}} \quad \textbf{(3.22)}$$

where F_{rr} is rolling resistance, h is the fraction of energy lost due to tire hysteresis, E is the linearly approximated elastic modulus of rubber, and t, s and r_w are the radial thickness, width and unloaded radius of the tire, respectively.

In terms of model implementation, if the sum of motor force and gravitational resistance is less than the rolling resistance (e.g. if the vehicle is on a very steep gradient), then rolling resistance is adjusted to exactly equal to the negative of this sum. This will cause the vehicle to remain stationary on a gradient it cannot climb. The model also does not permit the vehicle to roll backwards down a hill.

3.4.1.4 Model Implementation

The acceleration model was built using a simple Excel spreadsheet (Figure 25). Each row in the spreadsheet represents one time step. The vehicle starts from standstill and accelerates depending on forces calculated in each time step. Gradability was estimated using the solver feature in Excel by setting a target speed and varying the gradient. The exact formula used in each cell is presented in Appendix A.

Time (s)	Speed (m/s)	Speed (km/h)	Wheel RPM	Wheel speed (rad/s)	Torque (Nm)	Motor Force (N)	Aero Drag Force (N)	Net Force (N)	Motor power (W)	Power draw (W)	Current (A)	Acc (m/s^2)			
0.0	0.0	0.0	0.0	0.0	750	2500	0	2383	0	0	0	3.40		Timestep (s)	0.5
0.5	1.7	6.1	54.2	5.7	723	2410	15	2278	4102	5127	34	3.25			
1.0	3.3	12.0	106.0	11.1	697	2323	58	2148	7735	9669	64	3.07		**Road Conditions**	
1.5	4.9	17.5	154.8	16.2	673	2242	124	2001	10904	13630	91	2.86		Gradient (%)	0%
2.0	6.3	22.7	200.3	21.0	650	2166	208	1841	13632	17039	114	2.63		Gradient (deg)	0.00
2.5	7.6	27.4	242.2	25.4	629	2096	304	1676	15950	19937	133	2.39		Gravitational resistance (N)	0.00
3.0	8.8	31.7	280.3	29.4	610	2033	407	1509	17900	22375	149	2.16		Tire normal force (N)	6867.00
3.5	9.9	35.6	314.6	32.9	593	1976	513	1346	19526	24408	163	1.92		Rolling resistance (N)	116.82
4.0	10.8	39.0	345.2	36.1	577	1925	617	1191	20873	26091	174	1.70			
4.5	11.7	42.1	372.3	39.0	564	1880	718	1045	21982	27477	183	1.49		**Results**	
5.0	12.4	44.8	396.0	41.5	552	1840	812	911	22892	28615	191	1.30		Max speed (km/h)	60.64
5.5	13.1	47.1	416.7	43.6	542	1805	900	789	23637	29546	197	1.13		Peak acceleration (m/s^2)	3.40
6.0	13.7	49.2	434.7	45.5	533	1776	979	680	24246	30308	202	0.97		Peak power (kW)	9.02
6.5	14.1	50.9	450.1	47.1	525	1750	1050	583	24744	30930	206	0.83		Peak current draw (A)	225.49
7.0	14.6	52.4	463.4	48.5	518	1728	1112	498	25151	31439	210	0.71			
7.5	14.9	53.7	474.7	49.7	513	1709	1167	425	25485	31856	212	0.61			

Figure 25 – Excerpt from spreadsheet containing the acceleration model

3.4.2 Drive Cycle Model

Like the acceleration model, the drive cycle model is also a time-step based numerical model. Unlike the acceleration model, the speed of the vehicle at each time step is specified in the drive cycle [41], and all other parameters are calculated from these parameters. The overall structure of the drive cycle model is shown on Figure 26.

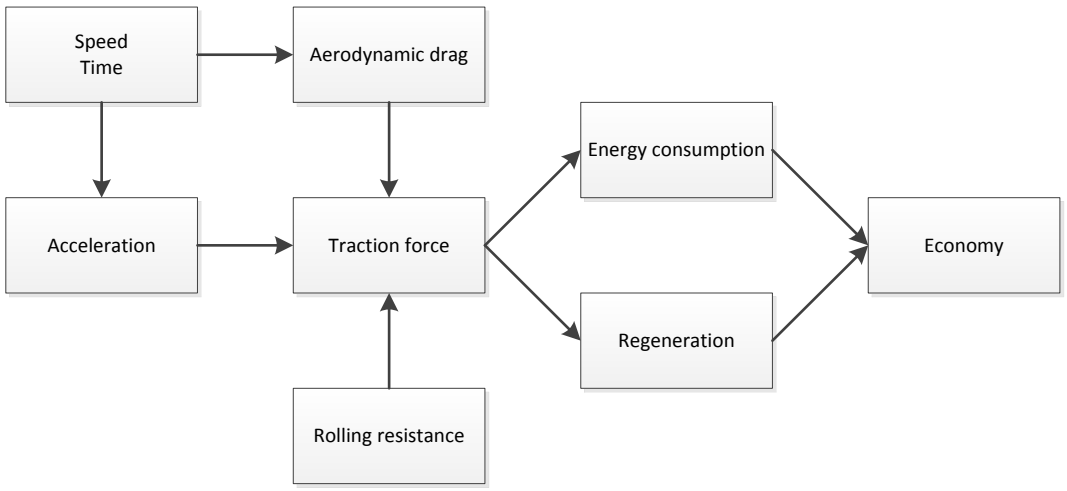

Figure 26 – Overview of the drive cycle model

The final goal of the model is to determine the amount of energy expended per unit distance travelled, from which the required battery capacity can be deduced based on range requirements. This leads to a rough estimate for battery mass and volume, which can then be used in packaging and vehicle dynamics analysis.

At each time step, the acceleration of the vehicle can be calculated by simply determining the rate of change of speed with respect to the previous time step. As a simplification, the acceleration between each time step is assumed to be constant. With acceleration known, the net force on the vehicle that caused this acceleration can then be calculated. By also calculating the aerodynamic drag force and applying rolling resistance at each time step as was done in the acceleration model, the remaining component of the net force, which is the tractive force, can be solved as follows:

$$F_t = F_{net} - (F_{drag} + F_{rr}) \quad \textbf{(3.23)}$$

If the tractive force is positive, then torque has been generated by the motor and energy has been withdrawn from the battery. If tractive force is negative, then the motor is assumed to have acted as a generator, converting kinetic energy of the vehicle back into electricity. The amount of energy flowing into or out of the battery at each time step is thus:

$$\Delta E = \begin{cases} F_t > 0 & \dfrac{F_t d}{e_{motor}} \\ F_t < 0 & -e_{regen} F_t d \end{cases} \quad \textbf{(3.24)}$$

where d is the distance travelled during the time step, e_{motor} is the average efficiency of the motor, e_{regen} is the average efficiency of the motor when used as a generator.

The sum of all ΔE over the drive cycle corresponds to the total energy consumed. Dividing this by the distance travelled over the drive cycle gives the energy economy of the vehicle in terms of energy consumed per unit distance travelled:

$$economy = \frac{\sum \Delta E}{\sum \mathrm{d}} \quad \textbf{(3.25)}$$

The required capacity of the batteries can be obtained by first multiplying economy by required range. Since it is generally unsafe to completely discharge a battery, the required capacity should be expanded such that the capacity calculated in the previous step corresponds to the usable energy content of a battery.

$$capacity = \frac{economy \times range}{\%\ maximum\ discharge} \quad \textbf{(3.26)}$$

3.5 Rollover Threshold Model

A static rollover model was built for rough estimation of rollover threshold under both longitudinal and lateral acceleration. Longitudinal acceleration is relevant in the case of three-wheeled vehicles because their tire contact patches form a triangle, which can be tripped by a combination of lateral and longitudinal acceleration.

Using front track, rear track, wheelbase, and coordinates of the CG, the rollover threshold model calculates the lateral rollover threshold for a range of longitudinal accelerations. The model also detects whether excessive longitudinal acceleration results in a nosedive or wheelie, which is possible given the small footprint of the vehicle.

Rollovers, nosedives, and wheelies occur when the net force vector acting on the center of gravity of the vehicle intersects the ground at a point outside the perimeter formed by its tire contact patches [30]. At equilibrium, the force vector points directly down, but under lateral or longitudinal acceleration, the force vector is deflected towards the direction of the acceleration.

To calculate this deflection, a coordinate frame of reference should first be defined. Using the SAE system, the origin of the coordinate frame of reference is defined as the point of intersection between the ground, the vehicle symmetry plane, and a vertical plane passing through the front wheel centers. The X, Y, and Z axes correspond to longitudinal, lateral, and vertical directions, respectively. X is positive towards the rear, Y is positive towards the right and Z is positive towards the top.

The CG of the vehicle is located at coordinates $(x_{CG}, 0, z_{CG})$. Under longitudinal acceleration a_x, the point of intersection between the force vector and the ground shifts by distance Δx, which can be calculated as follows:

$$\frac{F_z}{F_x} = \frac{mg}{ma_x} = \frac{z_{CG}}{\Delta x}$$

$$\Delta x = \frac{z_{CG}}{g} a_x \tag{3.27}$$

The x coordinate of the force vector intersection point, x_i, is thus located at $x_{CG} + \Delta x$. If x_i is less than zero (i.e. forward of the front wheel center), the vehicle experiences a nosedive. If x_i is greater than the wheelbase, then the vehicle experiences a wheelie. At x_i, the distance from the vehicle centerline to the line formed between the front and rear tires on one side of the vehicle can be calculated as follows:

$$\Delta y = \left(\frac{\frac{1}{2} T_r - \frac{1}{2} T_f}{L_{wb}} \right) x_i + \frac{1}{2} T_f \tag{3.28}$$

where T_f is front track, T_r is rear track, and L_{wb} is the wheelbase. This formula is derived from the equation of a straight line connecting the front and rear tires on one side of the vehicle with the vehicle centerline as the x axis. The value of Δy is in fact also the maximum lateral deflection of the intersection point between the net force vector and the ground

before the vehicle rolls over. The lateral acceleration that causes this deflection can be calculated as follows:

$$\frac{mg}{ma_y} = \frac{z_{CG}}{\Delta y}$$

$$a_y = \frac{g}{z_{CG}} \Delta y \quad \textbf{(3.29)}$$

Given a range of a_x values, a corresponding maximum a_y before rollover can thus be calculated from each a_x value. It's worthwhile to note that the dynamic rollover behavior of three-wheeled vehicles is markedly different from that of four-wheeled counterparts. For a three wheel configuration with two wheels in the front and two wheels in the back, the vehicle becomes more vulnerable to rollover when accelerating or driving uphill. For a one-front two-rear configuration, the vulnerability arises when braking or driving downhill.

3.6 Steering Response Model

As discussed in section 2.3.2.3, it is possible for an otherwise oversteer vehicle to behave like an understeer vehicle if all of its wheels are independently steerable. However, a limit still needs to be placed on how far rearward the CG should be allowed to avoid overloading the steer-by-wire system. Since little information is currently available on the steer-by-wire system, the CG location requirement is specified in the context of avoiding a low critical velocity assuming the vehicle was front-wheel-steered. The purpose of the steering response model is to determine whether the simplified vehicle is understeer, neutral, or oversteer, and its critical speed if it is oversteer. Later on, the model can be modified to incorporate the effect of a rear-wheel steering angle to aid in the development of a control algorithm for the steer-by-wire system.

The steering response model idealizes the vehicle as a bicycle, in that if an axle has two wheels, the forces and moments generated by the two wheels are added up and treated as if they were a single wheel. Unlike real bicycles, the idealized bicycle does not roll. Its body is treated as a point mass located at its CG, and forces generated by the two wheels act upon this point mass, driving its motion. Derivation of the model in this thesis will be brief, and readers are referred to Jazar (2008) [31] for a full derivation.

The motion of a steered vehicle on a 2D plane is derived from the Newton-Euler equations of motion:

$$F_x = m\dot{v}_x - mrv_y \tag{3.30}$$

$$F_y = m\dot{v}_y + mrv_x \tag{3.31}$$

$$M_z = \dot{r}_z I_z \tag{3.32}$$

where v_x, v_y r, and I_z are the vehicle's forward velocity, lateral velocity, yaw rate and moment of inertia about z, respectively. F_x is produced by the powertrain, while F_y and M_z result from lateral forces from the tires generated through sideslip. For a front-wheel-steering vehicle, tire forces are described as follows:

$$F_y = \left(-\frac{a_1}{v_x}C_{\alpha f} + \frac{a_2}{v_x}C_{\alpha r}\right)r - \left(C_{\alpha f} + C_{\alpha r}\right)\beta + C_{\alpha f}\delta \tag{3.33}$$

$$M_z = \left(-\frac{a_1^2}{v_x}C_{\alpha f} - \frac{a_2^2}{v_x}C_{\alpha r}\right)r - \left(a_1 C_{\alpha f} - a_2 C_{\alpha r}\right)\beta + a_1 C_{\alpha f}\delta \tag{3.34}$$

where a_1 and a_2 are the longitudinal distances between the CG and front and rear axles, respectively, $C_{\alpha f}$ and $C_{\alpha r}$ are the total tire cornering stiffness on the front and rear axles, respectively, β is tire sideslip angle, and δ is tire steer angle. These forces can be rewritten in a simplified form as follows:

$$F_y = C_r r + C_\beta \beta + C_\delta \delta \tag{3.35}$$

$$M_z = D_r r + D_\beta \beta + D_\delta \delta \tag{3.36}$$

where:

$$C_r = -\frac{a_1}{V_x}C_{\alpha f} + \frac{a_2}{v_x}C_{\alpha r} \tag{3.37}$$

$$C_\beta = -\left(C_{\alpha f} + C_{\alpha r}\right) \tag{3.38}$$

$$C_\delta = C_{\alpha f} \tag{3.39}$$

$$D_r = -\frac{a_1^2}{v_x}C_{\alpha f} - \frac{a_2^2}{v_x}C_{\alpha r} \tag{3.40}$$

$$D_\beta = -\left(a_1 C_{\alpha f} - a_2 C_{\alpha r}\right) \quad \textbf{(3.41)}$$

$$D_\delta = a_1 C_{\alpha f} \quad \textbf{(3.42)}$$

For the purposes of determining critical velocity, the vehicle can be assumed to under steady-state cornering, such that $\dot{v}_x$, $\dot{v}_y$ and $\dot{r}_z$ are all equal to zero. This simplifies equations (3.30) - (3.32) to:

$$F_x = -mrv_y \quad \textbf{(3.43)}$$

$$F_y = mrv_x \quad \textbf{(3.44)}$$

$$M_z = 0 \quad \textbf{(3.45)}$$

Equating equations (3.35)-(3.36) with (3.44)-(3.45) gives:

$$F_x = -mrv_y \quad \textbf{(3.46)}$$

$$C_r r + C_\beta \beta + C_\delta \delta = mrv_x \quad \textbf{(3.47)}$$

$$D_r r + D_\beta \beta + D_\delta \delta = 0 \quad \textbf{(3.48)}$$

v_x is equivalent to:

$$v_x = Rr \quad \textbf{(3.49)}$$

where R is the radius of the turn. Using this definition, equations (3.46)-(3.48) become:

$$F_x = -\frac{m}{R} v_x v_y \quad \textbf{(3.50)}$$

$$C_\beta \beta + (C_r v_x - m v_x^2)\frac{1}{R} = -C_\delta \delta \quad \textbf{(3.51)}$$

$$D_\beta \beta + D_r v_x \frac{1}{R} = -D_\delta \delta \quad \textbf{(3.52)}$$

Here, $\frac{1}{R}$ is the curvature of the turn and can be rewritten as κ. Writing equations (3.51) and (3.52) in matrix form gives:

$$\begin{bmatrix} C_\beta & C_r v_x - m v_x^2 \\ D_\beta & D_r v_x \end{bmatrix} \begin{bmatrix} \beta \\ \kappa \end{bmatrix} = \begin{bmatrix} -C_\delta \\ -D_\delta \end{bmatrix} \delta \quad \textbf{(3.53)}$$

Solving for β and κ gives:

$$\begin{bmatrix}\beta\\ \kappa\end{bmatrix} = \begin{bmatrix}\dfrac{D_\delta(C_r m v_x) - D_r C_\delta}{D_r C_\beta - C_r D_\beta + m v_x D_\beta}\\ \dfrac{C_\delta D_\beta - C_\beta D_\delta}{v_x\left(D_r C_\beta - C_r D_\beta + m v_x D_\beta\right)}\end{bmatrix}\delta \tag{3.54}$$

From this solution, we can obtain the curvature response S_κ:

$$S_\kappa = \frac{\kappa}{\delta} = \frac{C_\delta D_\beta - C_\beta D_\delta}{v_x\left(D_r C_\beta - C_r D_\beta + m v_x D_\beta\right)} \tag{3.55}$$

For a given forward speed, the curvature response is the amount of increase in the steady-state curvature of the turn per unit increase in steering angle. The curvature response equation can be manipulated to isolate a useful variable called the stability factor K, as follows:

$$S_\kappa = \frac{1}{v_x\left(\dfrac{D_r C_\beta - C_r D_\beta}{C_\delta D_\beta - C_\beta D_\delta} + \dfrac{m v_x D_\beta}{C_\delta D_\beta - C_\beta D_\delta}\right)}$$

$$S_\kappa = \frac{1}{l + \dfrac{m v_x^2 D_\beta}{C_\delta D_\beta - C_\beta D_\delta}} = \frac{1}{l}\frac{1}{1 + \dfrac{m}{l}\dfrac{D_\beta}{C_\delta D_\beta - C_\beta D_\delta} v_x^2}$$

$$S_\kappa = \frac{1}{l}\frac{1}{1 + K v_x^2} \tag{3.56}$$

The formula for K is:

$$K = \frac{m}{l}\frac{D_\beta}{C_\delta D_\beta - C_\beta D_\delta} \tag{3.57}$$

where l is the wheelbase of the vehicle. In expanded form:

$$K = \frac{m}{l}\left(\frac{a_2}{C_{\alpha f}} - \frac{a_1}{C_{\alpha r}}\right) \tag{3.58}$$

The sign of K indicates whether steering characteristic is understeer, oversteer, or neutral. The effect of K on curvature response can be seen on Figure 27. If $K > 0$, S_κ decreases with increasing speed and the vehicle is understeer. If $K = 0$, S_κ is constant and the vehicle is neutral steer. If $K < 0$, S_κ increases with speed and the vehicle is oversteer.

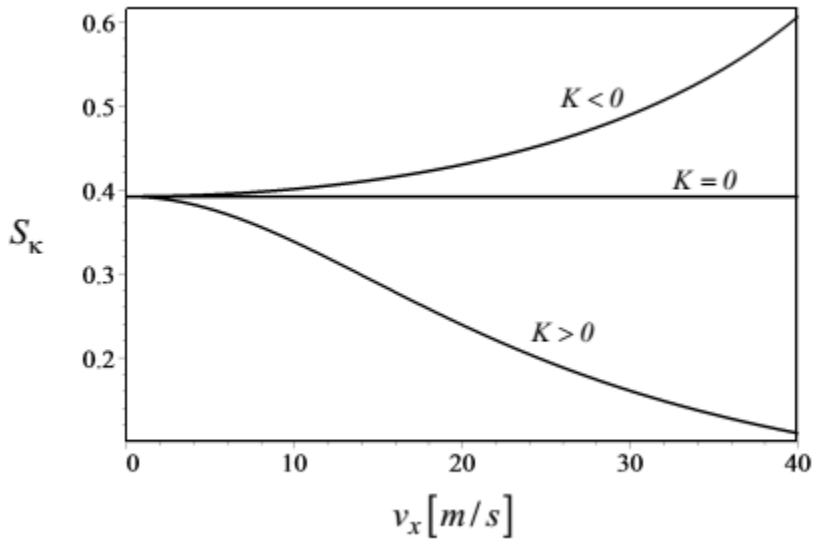

Figure 27 – Curvature response of an understeer, neutral, and oversteer vehicle [31]

If the vehicle is oversteer, there is a vertical asymptote in the graph of S_κ located at:

$$v_{crit} = \sqrt{-\frac{1}{K}} \tag{3.59}$$

As v_x approaches v_{crit}, S_κ approaches infinity and the steering response becomes so sensitive that the vehicle is a risk of losing control even with minimal steering input. It should be noted here that this result is only applicable for a front-wheel-steered vehicle. If the vehicle is all-wheel-steer, equations (3.35) and (3.36) would become:

$$F_y = C_r r + C_\beta \beta + C_{\delta f}\delta_f + C_{\delta r}\delta_r \tag{3.60}$$

$$M_z = D_r r + D_\beta \beta + D_{\delta f}\delta_f + D_{\delta r}\delta_r \tag{3.61}$$

An algorithm would then be needed to control δ_f and δ_r to achieve the desired steering response, and the accuracy and speed with which these can be controlled would determine the rearmost limit of CG position. This can be subject for future work on the project, but for now, it is sufficient to position the CG so that the v_{crit} of an equivalent front-wheel-steered vehicle is well above the vehicle maximum speed.

3.7 Summary

In this chapter, tools were developed to drive the design process along specification guidelines created in Chapter 2. The list of tools developed is shown on Table 10. Unfortunately, the application scope of these tools do not account for all major space-taking components of the vehicle, in particular the structure and storage space (Figure 14). Furthermore, the quality of information currently available for use as calculation input is rather crude, such as in the case of tire cornering stiffness, which is largely unknown. In the next chapter, the tools that have thus far been developed will be employed in the design of a partial concept using the limited information that is currently available for the purposes of demonstrating the application of these tools.

Chapter 4 Partial Design Concept

At this point in design, there is still much missing information that is needed to complete a full vehicle concept with all major space-taking components included. As can be seen on Figure 14, two of the largest space-taking components, the structure and storage, are still not accompanied by appropriate specifications and design tools. In spite of this, it is still possible to generate a partial concept to demonstrate the application of the tools developed in the previous chapter.

The design process will be broken down into three steps. First, major space-taking components such as the crumple zone and batteries will be sized. Second, the major space-taking components will be arranged into a package with the smallest form factor possible. Finally, basic dynamics calculations will be performed to evaluate the stability of this package and iteratively adjust it until specifications are met.

4.1 Crumple Zone Sizing

Test conditions from the US NCAP front and side collisions are used as inputs for the crash structure models. In the front impact test, the goal is to limit peak cabin acceleration to 46 g. In the side impact test, the goal is to limit average occupant acceleration to 57 g. The vehicle is assumed to have a weight of 700 kg and the crush efficiency of its front structure is assumed to be 0.9. The outer shell of its doors is assumed to be sufficiently rigid to develop 280,000 N of force upon the crash barrier.

The crash conditions and results are shown on Table 13. For a frontal impact, the crash structure model suggests that a front crumple zone of 300 mm is sufficient. For side impact, the thickness of the door cushion region is estimated at 160 mm. For comfort, a gap of 20 mm is added between the occupant and the door cushion. The thickness of the outer shell of the door is assumed to be another 20 mm. The overall door thickness is thus 200 mm. A time history of the side impact test can be seen on Figure 28.

Table 13 – Inputs and outputs from crash structure models

Crash conditions		
	Front	**Side**
Vehicle mass	700 kg	
Barrier mass	N/A	1370 kg
Door crush load	N/A	280,000 N
Crush efficiency	0.9	N/A
Impact speed	56 km/h	62 km/h*
Acceleration target	450 m/s^2 (46 g)**	496 m/s^2 (51 g)***
Crash structure dimensions		
Length X	300 mm	Occupant length
Length Y	Vehicle width	Shell: 20 mm Cushion: 160 mm Gap: 20 mm
Length Z	Hood height	Occupant height

* Absolute speed of barrier
** Peak cabin acceleration
*** Occupant acceleration

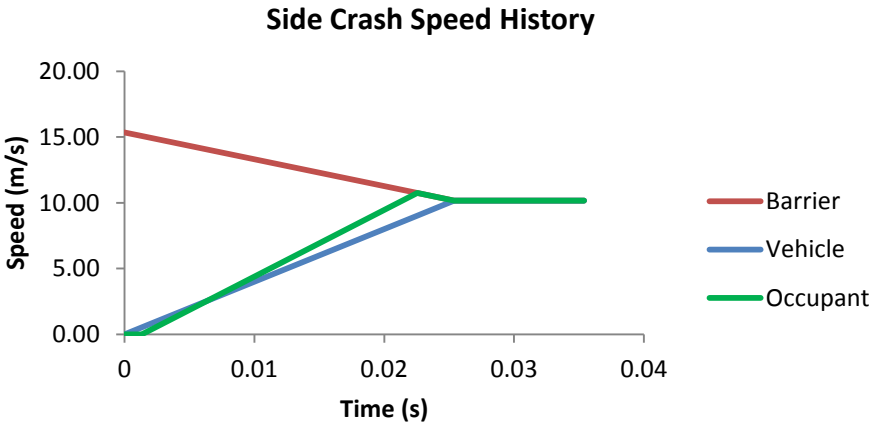

Figure 28 – Side crash history of partial concept

4.2 Motor and Battery Sizing

The results of motor and battery sizing are shown on Table 14. Of most interest to vehicle packaging is the size and weight of the batteries required to deliver the required range. Assuming a specific energy of 130 Wh/kg and energy density of 200 Wh/L, typical of most lithium ion batteries, the battery pack would weigh 111 kg with a volume of 72 L. For now, it is assumed that the dimensions of the battery pack can be anything so long as it has a volume of 72 L, although limitations would be added during actual battery selection.

Table 14 – Drivetrain parameters

Area	Variable	Value
Motor	Nominal torque	210 Nm
	Nominal speed	600 RPM
	Maximum speed	1100 RPM
	Average energy efficiency	85%*
	Average regeneration efficiency	5%*
Batteries	Battery capacity	14.4 kWh
	Max discharge depth	80%
	Usable capacity	11.5 kWh
	Battery weight	111 kg
	Battery volume	72 L
Tires	Diameter	600 mm
	Width	150 mm
	Radial thickness	50 mm
	Hysteresis coefficient	0.2*
	Elastic modulus	13.1 MPa*
Aerodynamics	Frontal area	2.25 m^2
	Drag coefficient	0.3*

* Value is assumed

The speed and acceleration performance of the vehicle is shown on Figure 29 and Figure 30. The vehicle has a top speed of about 70 km/h on flat ground, and can reach that speed in just over 10 seconds. The acceleration curve of Figure 30 shows that the vehicle is able

to complete the NYCC drive cycle and keep up with accelerating traffic as discussed in Section 2.3.1.2.

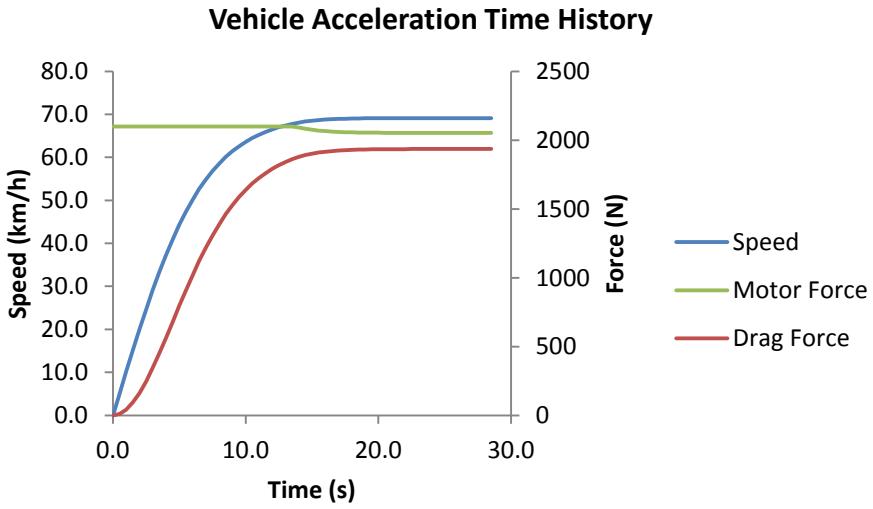

Figure 29 – Speed history of accelerating partial concept

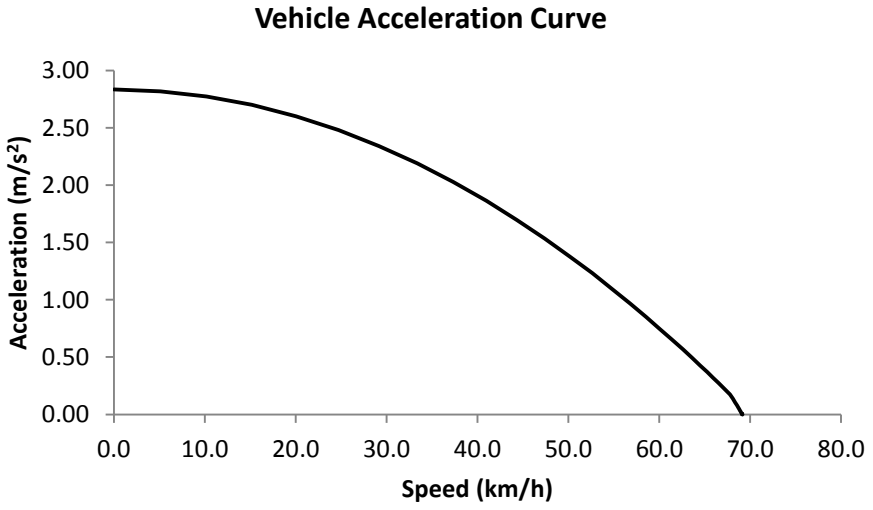

Figure 30 – Acceleration curve of partial concept

Table 15 – Gradability and range performance of partial concept

Parameter	Value
Gradability at 50 km/h	20%
Gradability before stall	51%
Energy economy (NYCC)	95 Wh/km
Energy economy (ECE15)	110 Wh/km
Range (NYCC)	121 km
Range (ECE15)	105 km

4.3 Packaging and Turning Performance

With the crumple zones and batteries sized, a partial vehicle package can be made by adding the occupant models and CWMs (Figure 31). Overall vehicle dimensions for the smallest form factor achieved is about 2.2 m in length, 1.5 m in width, and 1.6 m in height. This allows for a wheelbase of 1.5 m and track of 1.4 m. When the front wheels are cambered at 45 degrees, the track increases to 1.8 m.

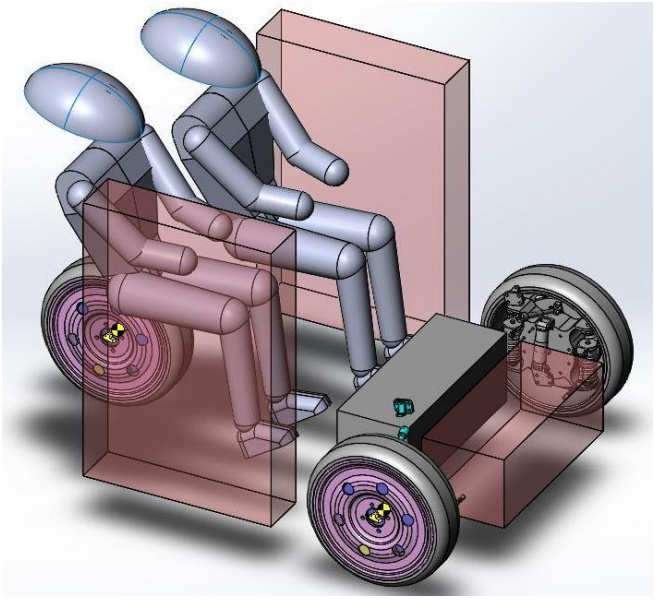

Figure 31 – Packaging of partial concept

Table 16 – Input parameters for turning performance models

Parameter	Value
Wheelbase	1.5 m
Track	1.4 m
Track (full camber)	1.8 m
CG height	0.4 m*
CG longitudinal distance from front axle	0.6 m*
Cornering stiffness per tire	28000 N/rad*
$C_{\alpha f}$	56000 N/rad
$C_{\alpha r}$	28000 N/rad

* Value is assumed

Since many components remain to be designed, it is not possible to determine the location of the CG to reasonable accuracy. Thus, it is assumed that the final CG position is 0.4 m from ground and 0.6 m rearward of the front axle. With this combination of wheelbase, track, and CG location, a rollover threshold profile can be obtained (Figure 32). Without any longitudinal acceleration, the vehicle has a rollover threshold of 1.54 g. However, if the vehicle accelerates too quickly while turning, the risk of rollover becomes much greater. Fortunately, since both steering and throttle are electronically actuated, it is possible to limit either or both to prevent rollover.

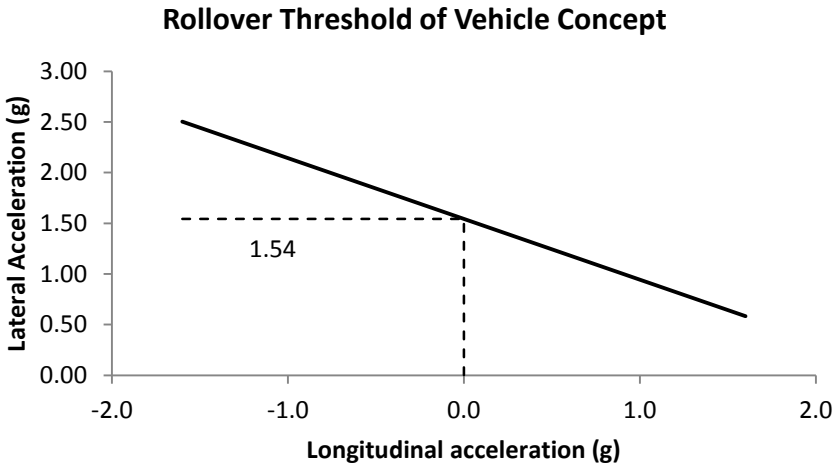

Figure 32 – Rollover threshold graph

Considering only the weight of the drivers, CWMs, and batteries, the vehicle weighs 360 kg and the longitudinal position of its CG is 0.68 m from the front axle. The heaviest component that is not accounted for is the structure, which is unlikely to have sufficient influence on the CG to bring it to the 1/3 wheelbase position required for neutral steer. Thus, assuming a final longitudinal CG position of 0.6 m rearward of front axle, an equivalent front-wheel-steered vehicle would be oversteer with a critical velocity of 88 km/h, as determined by the steering response model.

Chapter 5
Conclusions and Future Work

5.1 Conclusions

This thesis documented the development of a three-wheeled electric urban vehicle in terms of requirements engineering (Chapter 2), rough calculation models for important vehicle parameters (Chapter 3), and the development of a partial concept (Chapter 4).

The specifications developed in Chapter 2 focuses on vehicle packaging, linear performance, and cornering dynamics. A summary of specifications developed can be found in Section 2.4. These specifications are accompanied by order-of-magnitude calculation tools developed in Chapter 3, which are then applied in the concept designed in Chapter 4. Although this particular specification-calculation-design chain is mostly complete, it is only one of many similar processes that need to be developed in order for the project to progress.

5.2 Future Work

Since the scope of the project is large and not fully defined, it is impractical to present a full list of all future work required for project completion. As well, it is largely up to the technology developers – the primary stakeholders of the project – to decide how the project should proceed. Nevertheless, some possibilities will be given in this section as project suggestions.

Perhaps the most obvious projects in the short term would be the development of specification-calculation-design chains for the vehicle structure and storage. Once these components are designed, all major components shown on Figure 14 will be accounted for, thus enabling the design of a full concept. Furthermore, many uncertain variables used as inputs for existing models will be known to greater certainty. An example would be the weight and CG location of the full vehicle, which is used in the rollover, linear performance, crashworthiness, and steering response models.

Before developing specifications for the storage, the usage scope of the vehicle should first be defined. Due to the small footprint of the vehicle, room for storage will likely be scarce, thus it is important to first determine the role and capacity of the storage area. Once the usage scope has been defined, it is straightforward to survey common cargo contents

brought by potential users of the vehicle for each trip purpose, and in turn derive its dimensional and loading specifications.

To develop specifications for the structure, three things need to be done. First, all possible load cases, including static, dynamic, and vibrational need to be determined. These load cases arise from possible events experienced by the vehicle during its lifetime, such as hitting a bump, cornering, towing, driving on rough road surface, and collisions. Second, the weights of all components attached to the structure, as well as their points of attachment need to be determined. Third, the CWMs need to be tested for their tolerance to structural flexing with respect to maintaining steering accuracy. Once all required information is in place, specifications for the structure can be determined in terms of strength required to avoid deformation, rigidity required to minimize steering error, and vibrational characteristics required to manage fatigue and occupant comfort.

As was done in this thesis, simple order-of-magnitude calculations can be developed for initial design of the structure. As suggested in Malen (2011) [34], these calculation can be as simple as treating the entire structure as a simply supported beam loaded in bending. More sophisticated models can be made by treating the structure as a network of simple beams and surfaces, each with its own stress calculation. Ultimately, finite element analysis can be used once the speed advantage of a simple exploratory model no longer outweighs the need for accuracy.

Aside from design of these components, another possible project would be refinement or replacement of existing calculation models once more information becomes available for use as model inputs.

All vehicle dynamics models, such as the acceleration, drive cycle, rollover and steering response models would benefit from the inclusions of tire characteristics such as rolling resistance, forces and moments generated under longitudinal slip, sideslip and camber, as well as the variation of these with normal load. This would enable the prediction of traction loss under linear acceleration and cornering and produce meaningful results in the steering response model.

Another possibility for refinement would be the modification of the steering response model to account for independent front and rear wheel steering. In this case, the single

steering angle δ in equation (3.53) would be replaced by independent front and rear steer angles in matrix form, $\begin{bmatrix}\delta_f \\ \delta_r\end{bmatrix}$, and algorithms can be developed to control δ_f and δ_r so that the vehicle would always exhibit understeer behavior.

Finally, once the design matures to a point where accuracy is favored over calculation speed, all models can be replaced with more sophisticated commercial software packages. The vehicle dynamics model can be replaced with multi-body simulation packages such as ADAMS, the crash models with large deformation finite element analysis packages such as LS-Dyna, and the occupant model with ergonomics packages like CATIA Vehicle Occupant Accommodation. Replacing with commercial packages does not make the original models obsolete, however, as the original models can be used to cross-check the often black-box results from commercial packages.

Appendix A – Equations Used in Models

Table A1 – Acceleration model

Wheel speed (rad/s)	$\omega = \frac{v}{r_w}$
Torque per motor (Nm)	$\tau = \begin{cases} \tau_{rated}, & \omega \leq \omega_{rated} \\ \tau_{rated} - \tau_{rated}\frac{\omega - \omega_{rated}}{\omega_{max} - \omega_{rated}}, & \omega > \omega_{rated} \end{cases}$
Motor force (N)	$F_{mot} = \frac{n\tau}{r_w}$
Drag force (N)	$F_{drag} = \frac{1}{2}\rho C_d A v^2$
Gravitational resistance (N)	$F_{grav} = mg\sin\theta$
Rolling resistance (N)	$F_{rr} \cong \frac{h}{4.4}\left(\frac{W^4 t}{E s r_w^2}\right)^{\frac{1}{3}}$
Net force (N)	$F_{net} = \begin{cases} F_{mot} - \left(F_{drag} + F_{grav} + F_{rr}\right), & F_{mot} - F_{grav} > F_{rr} \\ 0, & F_{mot} - F_{grav} \leq F_{rr} \end{cases}$
Acceleration (m/s^2)	$a = \frac{F_{net}}{m}$

Table A2 – Drive cycle model

Acceleration (m/s^2)	$a = \frac{v_n + v_{n-1}}{\Delta t}$
Distance over time step (m)	$d = \Delta t \frac{v_n + v_{n-1}}{2}$
Drag force (N)	$F_{drag} = \frac{1}{2}\rho C_d A v^2$
Rolling resistance (N)	$F_{rr} = \begin{cases} 0, & \frac{v_n + v_{n-1}}{2} = 0 \\ \frac{h}{4.4}\left(\frac{W^4 t}{E s r_w^2}\right)^{\frac{1}{3}} & \frac{v_n + v_{n-1}}{2} > 0 \end{cases}$
Traction force (N)	$F_t = ma + F_{drag} + F_{rr}$
Energy flow (J)	$\Delta E = \begin{cases} -\frac{F_t d}{e_{motor}} & F_t > 0 \\ \frac{F_t d}{e_{regen}} & F_t \leq 0 \end{cases}$

Bibliography

[1] J. Banhart and D. Weaire, "On the Road Again: Metal Foams Find Favor," *Physics Today,* pp. 37-42, 2002.

[2] W. Abramowicz, "Thin-Walled Structures as Impact Energy Absorbers," *Thin-Walled Structures,* pp. 91-107, 2002.

[3] D. Ullman, The Mechanical Design Process, New York: McGraw-Hill, 2002.

[4] V. D. Bhise, Ergonomics in the Automotive Design Process, CRC Press: Boca Raton, 2012.

[5] Society of Automotive Engineers Inc., SAE Handbook, Warrendale: Society of Automotive Engineers Inc., 2009.

[6] R. Q. Riley, Alternative Cars in the 21st Century, 2nd Ed., Warrendale: Society of Automotive Engineers, 2004.

[7] J. W. McClenahan and H. J. Simkowitz, "The Effect of Short Cars on Flow and Speed in Downtown Traffic: A Simulation Model and Some Results," *Transportation Sicence,* vol. 3, no. 2, 1969.

[8] R. A. Weant, Parking Garage Planning and Operation, Westport: Eno Foundation for Transportation, Inc., 1978.

[9] Carl Walker, Inc., "Parking Structure Design Guidelines," Carl Walker Inc., Tempe, 2014.

[10] Institute of Transportation Engineers, "Guidelines for the Design and Application of Speed Humps," ITE Journal, 1993.

[11] American Association of State Highway and Transportation Officials, Geometric Design of Highways and Streets, Washington DC: American Association of State Highway and Transportation Officials, 2004.

[12] National Highway Safety Administration, "NHTSA Vehicle Parameter Database," University of Michigan, 2014. [Online]. Available: http://mreed.umtri.umich.edu/mreed/downloads.html. [Accessed 30 May 2014].

[13] T. Franke and J. F. Krems, "What Drives Range Preferences in Electric Vehicle Users?," *Transport Policy,* vol. 30, no. November, pp. 56-62, 2013.

[14] N. S. Pearre, W. Kempton, R. L. Guensler and V. V. Elango, "Electric Vehicles: How Much Range is REquired for a Day's Driving?," *Transportation Research Part C: Emerging Technologies,* vol. 19, no. 6, pp. 1171-1184, 2011.

[15] Infas, DLR, "Mobilitat in Deutschland: Ergebnisbericht," 2010. [Online]. Available: http://mobilitaet-in-deuchland.de/02_MiD2008/publikationen.htm.

[16] D. Zumkeller, P. Vortisch, M. Kagerbauer, B. Chlond, T. Streit and M. Wirtz, "Deutsches Mobilitätspanel (MOP) - wissenschaftliche Begleitung und erste Auswertungen," 2011.

[17] Öko-Institut, "Autos unter Strom," 2011. [Online]. Available: http://www.oeko.de/oekodoc/1283/2011-413-de.pdf.

[18] TÜV Rheinland, "Results of the Representative Survey on the Acceptance of Electric Cars," 2011. [Online]. Available: http://www.dincertco.de/web/media_get.php?mediaid=35741&fileid=86473&sprachid=2.

[19] I. Bunzeck, C. Feenstra and M. Paukovic, "Preferences of Potential Users of Electric Cars Related to Charging - A Survey in Eight EU Countries," 2011.

[20] C. Giffi, J. Vitale Jr., M. Drew, Y. Kuboshima and M. Sase, "Unplugged: Electric Vehicle Realities Verses Consumer Expectations," 2011.

[21] J. Krumm, "How People Use Their Vehicles: Statistics from the 2009 National Household Travel Survey," Society of Automotive Engineers, 2012.

[22] VDE, "E-Mobility 2020," 2010. [Online]. Available: http://www.vde.com/de/E-Mobility/Seiten/VDEStudieEMobility2020.aspx.

[23] ADAC, "ADAC Elektromobilität 2013 - Umfrage im Auftrag des ADAC Technik Zentrums," 2013. [Online]. Available: http://www.konferenz-elektromobilitaet.de/programm/vortraege/Umfrage-Elektromobilitaet-2013.pdf.

[24] S. Bronchard, M. McGuiness, C. Narich, M. Noom, C. Raut, M. Schutz, M. Stark, P. Ubbink, M. Viglino and A. Vos, "Plug-in Electric Vehicles - Changing Perceptions Hedging Bets," 2011.

[25] Zpryme, "The Electric Vehicle Study," 2010.

[26] A. Mehar, S. Chandra and S. Velmurugan, "Speed and Acceleration Characteristics of Different Types of Vehicles on Multi-Lane Highways," *European Transport,* no. 55, 2013.

[27] G. Long, "Acceleration Characteristics of Starting Vehicles," in *Transportation Research Board 79th Annual Meeting*, Washington DC, 2000.

[28] W. J. Stein and T. R. Neuman, "Mitigation Strategies for Design Exceptions," US Department of Transportation, Washington DC, 2007.

[29] M. C. Walz, "Trends in the Static Stability Factor of Passenger Cars, Light Trucks and Vans," National Highway Traffic Safety Administration, Washington DC, 2005.

[30] National Highway Traffic Safety Administration, *Rollover Resistance - Final Policy Statement,* Washington D.C., 2003.

[31] R. N. Jazar, Vehicle Dynamics: Theory and Application, New York: Springer, 2008.

[32] Global New Car Assessment Programme, "NCAP Brochure for ESV Conference," June 2011. [Online]. Available: http://www.globalncap.org/wp-content/uploads/2013/07/esv_brochure.pdf. [Accessed July 2014].

[33] L. L. Hershman, "The U.S. New Car Assessment Program (NCAP): Past, Present and Future," in *International Technical Conference on the Enhanced Safety of Vehicles (ESV)*, Amsterdam, Netherlands, 2001.

[34] D. E. Malen, Fundamentals of Automobile Body Structure Design, Warrendale: SAE International, 2011.

[35] H. Chan, J. R. Hackney, R. M. Morgan and H. E. Smith, "An Analysis of NCAP Side Impact Crash Data," National Highway Traffic Safety Administration, 1999.

[36] J. J. Swearingen, "Determination of Centers of Gravity of Man," Federal Aviation Agency, Oklahoma, 1962.

[37] I. Husain, Electric and Hybrid Vehicles - Design Fundamentals, Boca Raton: CRC Press, 2011.

[38] I. Evans, "The Rolling Resistance of a Wheel with a Solid Rubber Tyre," *British Journal of Applied Physics,* vol. 5, no. 5, pp. 187-188, 1953.

[39] A. M. Kwarciak, M. Yarossi, A. Ramanujam, T. A. Dyson-Hudson and S. A. Sisto, "Evaluation of Wheelchair Tire Rolling Resistance Using Dynamometer-based Coasst-down Tests," *Journal of Rehabilitation Research & Devleopment,* vol. 46, no. 7, pp. 931-938, 2009.

[40] M. Veeramurthy, J. Ju, L. L. Thompson and J. D. Summers, "Optimization of a Non-pneumatic Tire for Reduced Rolling Resistance," in *ASME International Design Engineering Technical Conferences & Computers and Information in Engineering Conference*, Washington DC, 2011.

[41] Environmental Protection Agency, "Dynamometer Drive Schedules," [Online]. Available: http://www.epa.gov/nvfel/testing/dynamometer.htm. [Accessed 2014].